



**The tTEM System**  
**System validation and comparison with PACES and ERT**  
**December 2019**

**The tTEM System - System validation and comparison with PACES and ERT - HGG - Aarhus University**





# The tTEM System

## System validation and comparison with PACES and ERT

December 2019

HydroGeophysics Group  
Department of Geoscience,  
Aarhus University, Denmark



## TABLE OF CONTENTS

<b>1 INTRODUCTION.....</b>	<b>3</b>
<b>2 THE TTEM-SYSTEM.....</b>	<b>5</b>
2.1 tTEM .....	5
2.2 Data Processing and Inversion.....	11
<b>3 METHODS – PACES AND ERT .....</b>	<b>13</b>
3.1 ERT .....	13
3.2 PACES.....	14
3.3 Resolution and Mapping Capability.....	15
3.4 Accumulated Clay Thickness.....	18
<b>4 TTEM TEST-SITE VALIDATION .....</b>	<b>20</b>
4.1 TEM Test Site .....	20
4.2 The Test Site Dataset .....	21
4.3 Validation Model Space .....	24
4.4 Validation Data Space.....	27
<b>5 MODEL RESOLUTION STUDY - TTEM, PACES, ERT .....</b>	<b>31</b>
5.1 The Modelling Scheme .....	31
5.2 Modelling Results and Discussion.....	33
<b>6 MAPPING EXAMPLES – METHODS COMPARISON .....</b>	<b>41</b>
6.1 tTEM and PACES – Oure Survey.....	41
6.2 tTEM and ERT – Vildbjerg, Stendal Mark, Javngyde .....	50
<b>7 DISCUSSION AND CONCLUSION .....</b>	<b>59</b>
<b>8 REFERENCES.....</b>	<b>61</b>
<b>APPENDIX 1 TEST SITE VALIDATION, MODEL SECTION</b>	
<b>APPENDIX 2 TEST SITE VALIDATION, DATA PLOTS</b>	
<b>APPENDIX 3 SETUP FILES</b>	
<b>APPENDIX 4 ADITIONAL MODEL SWEEPS</b>	



## Authors

Ph.D. Nikolaj Foged,  
Ph.D., Associate Prof. Anders Vest Christiansen.

Aarhus University, Department of Geoscience, HydroGeophysics Group  
Aarhus, Denmark, November 2019.

The research work presented in this report regarding validation of the tTEM method and comparison with other geophysical methods was primarily carried out in the framework of *GeoFysikSamarbejdet* (GFS), which is a collaboration between The Danish Environmental Protection Agency and the Department of Geoscience, Aarhus University.

The main development of the tTEM system was carried out within the research projects rOpen (Open landscape nitrate retention Mapping, Innovation fund Denmark), MapField (Field-scale mapping for targeted N-regulation and management, Innovation fund Denmark), and TopSoil (EU Inter-reg IV project).

## Acronyms

Acronyms	
ACT	Accumulated Clay Thickness
AEM	Airborne ElectroMagnetics
ATV	All-Terrain Vehicle
DC-methods	Geophysical methods that inject electrical current in the ground using electrodes with galvanic contact to the ground
DOI	Depth of Investigation
EM-methods	Electromagnetic methods which induce electrical currents in the ground through the principle of electromagnetic induction
ERT	Electrical Resistivity Tomography, which is also often referred to as MEP or CVES using other abbreviations. Here only ERT is used.
GCM	Ground Conductivity Meter (also referred to as EMI with another abbreviation).
GFS	GeoFysikSamarbejdet, collaboration between The Danish Environmental Protection Agency and the Department of Geoscience, Aarhus University
HGG	The HydroGeophysics Group at the Department of Geoscience, Aarhus University
IP	Induced Polarization
LCI	Laterally Constrained Inversion
PACES	Pulled Array Continuous Electrical Soundings
SCI	Spatially Constrained Inversion
TEM	Transient Electromagnetic
tTEM	Towed TEM
WalkTEM	Ground based and stationary TEM-system developed at HGG, Aarhus University



## 1 INTRODUCTION

The tTEM system is a compact, highly efficient towed TEM-system, designed for detailed 3D geophysical mapping of the shallow subsurface. This report first provides a comprehensive geophysical validation of the tTEM-system at its present stage, then a synthetic model resolution study is presented, and last we show several field comparison examples with the two DC-methods PACES and ERT, which have been widely used for shallow geophysical mapping in Denmark.



Figure 1. The tTEM system in action.

The tTEM validation part is based on repeated measurements from the Danish TEM test site and is performed by comparing both the resulting models, as well as comparing repeated data, directly. The validation serves to examine both the repeatability of the tTEM system, and the match to the test site reference section. All references to the “test-site” in this report refers to the Danish TEM test-site, located west of Aarhus close the village Lyngby.

In the modelling resolution study part, we examine the tTEM-system’s ability to resolve different layered resistivity models in a controlled environment where the *true model* is known. This modelling resolution study also includes comparisons to PACES and ERT so differences in resolution capability can be examined.



The third part of the report holds tTEM mapping examples, with comparisons to PACES and ERT results on survey scale in the form of resistivity sections, mean resistivity maps, and accumulated clay thickness maps.

This report is a strictly geophysical validation of the tTEM-system and does not touch upon geological interpretation of the tTEM mapping results, nor does it focus on comparisons to boreholes with lithological information. *Case story* papers based on tTEM mapping results with geological interpretations are available, and listed in the reference section, chapter 8.

The structure of the report is as follows: Chapter 2, provides a description of the tTEM system including some technical details, and gives a description of the standard processing and inversion scheme for tTEM-data. Chapter 3 gives a brief introduction to the PACES and ERT methods, a general description of the differences between DC- and TEM-methods with respect to resolution capability, and provide a short introduction to the ACT concept applied to the resistivity models in the later examples. Chapter 4, 5, and 6 contains the three main parts: the tTEM test site validation, the modelling resolution study, and the different field examples. Finally, the main results are summarized and discussed in chapter 7. Key references and supplementary literature for the different subjects/sections are listed in the reference section (chapter 8), while the appendixes hold additional plots from the test site validation and additional model sections for the resolution study.



## 2 THE TTEM-SYSTEM

### 2.1 TTEM

The tTEM-system is a towed, ground-based, transient electromagnetic system, designed for highly efficient data collection and detailed 3D geophysical and geological mapping of the shallow subsurface: the upper ~80 m. The present layout of the tTEM system is shown in Figure 1 and Figure 2. The main development of the tTEM-system was conducted in 2016-2018, building on the high expertise and experience within the HGG-group regarding all aspects of the TEM-method, from instrument design, testing and calibration, to data surveying, processing, and inversion of EM-data. Initially the design goal focused on resolving the top 50 m, but it turned out that the system was capable of resolving down to around 60-80 m.

The tTEM system also comes in a FloaTEM version operating on water and a SnowTEM version operating on snow and ice surfaces (see Figure 3). In this report, we focus on the standard tTEM-system, operating on land.

The tTEM-system (Figure 2) consists of an ATV, carrying the instrumentation and towing the transmitter frame (Tx coil) and the receiver coil (Rx coil) in an off-set configuration. The Tx and Rx coils are mounted on sleds for a smooth ride over rough fields/terrain. The frame and sleds are built of non-electrically conductive fiberglass and composite materials and are assembled with 3D printed, carbon strengthened, parts.

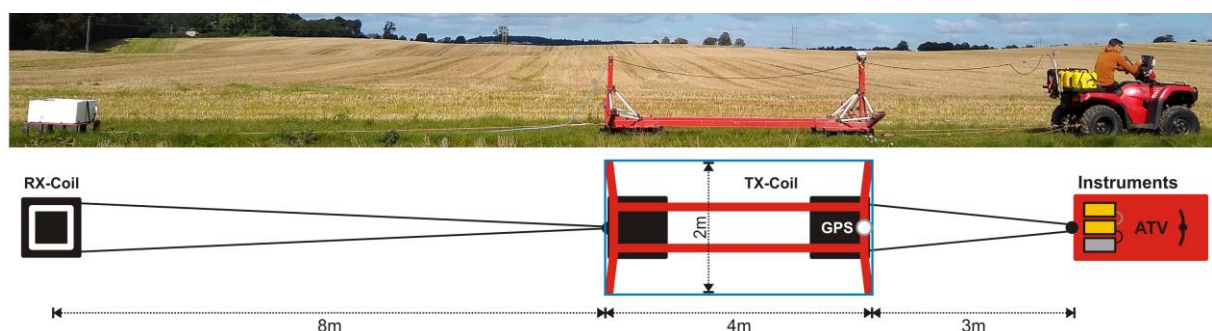


Figure 2. Layout of the tTEM system 2019.

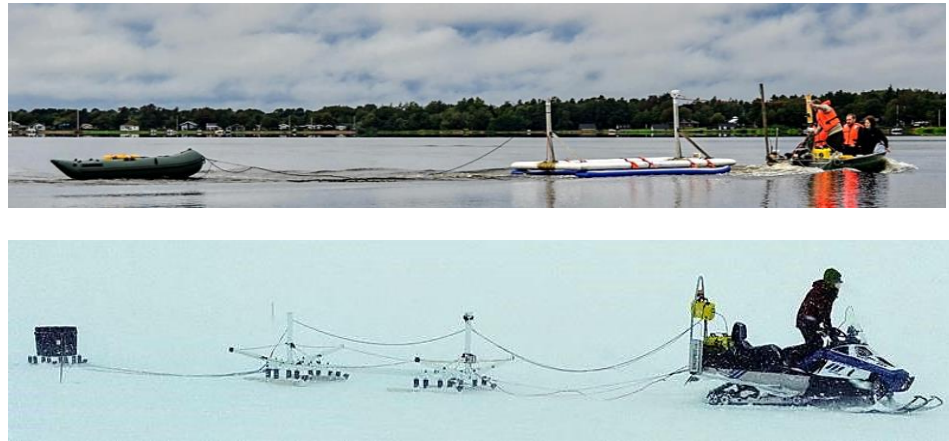


Figure 3. FloatTEM (top) and SnowTEM (Bottom).

The operational speed of the tTEM system is up to 20 km/h depending on the terrain and surface conditions. Popularly speaking, if the area is accessible with an ATV and there is at least a 2 m clearing for the frame, we can perform the tTEM mapping. When surveying on farmland, the driving tracks in the fields are used as driving guides to minimize crop impact, resulting in a line spacing of 15-25 m. Depending on field conditions and line density, the production rate is approximately 1 km<sup>2</sup> per day = 100 hectares/day, spanning from ~150 Ha/day in good conditions and ~50 Ha/day if conditions are poor.

Navigation and data collection are monitored and controlled by the driver using a tablet PC. This navigation software provides a real time display of the survey path, line numbers, status parameters, and various alarms from the instrumentation. Pre-planned survey lines and GIS maps can also be loaded into the navigation system. The geographical position of the data is recorded by one SBAS (Satellite Based Augmentation System) GPS placed on the Tx-frame. In later data processing, the GPS data are lag-corrected to position the data/resistivity model in-between the transmitter and receiver loops.

The tTEM system is operated by one person, but a second person is normally needed to assist with mobilization/demobilization, on-site survey planning, data quality control, and field safety. Mobilization as well as demobilization is quite fast and takes less than 20 min. Transportation wise, the 2 × 4 m<sup>2</sup> frame fits on a long car trailer. Placing the ATV in the back of the van makes transportation a single car job. Additionally, the system can be disassembled and palletized for longer transportation and shipment.



*Figure 4. The tTEM system packed on the transport trailer. The ATV and all instrumentation is inside the van.*

### **Design and Development History**

The development of the tTEM system started in 2015 and was initiated because of the lack of a geophysical method/instrument that could provide detailed 3D resistivity information in the upper ~50 m of the subsurface with fast and cost-effective data collection over relatively large areas. Large-scale 3D structural information is essential for building detailed hydrological models of the subsurface. These detailed models are important for a wide range of near-surface applications such as raw-material mapping, point source pollution mapping, climate adaptation, and nitrate retention assessments on field scale.

Existing geophysical tools that can be considered for a detailed 3D resistivity mapping task are: Ground conductivity meter (GCM), Airborne EM (e.g. SkyTEM), ERT, and PACES, but they all have downsides. For towed GCM instruments the mapping efficiency is good, but the surveying depth is limited to 7-10 m. ERT in a profile layout can provide the needed vertical and lateral resolution along the profile, but obtaining 3D data over larger areas is extremely time consuming. AEM provides a very efficient data collection, but the resolution in the upper 50 m is limited compared to ERT and GCM. Furthermore, the AEM lateral resolution is limited, due a typical line spacing of 200-300 meters, and a relatively large footprint. Operation/mobilization costs are also relatively high for an AEM survey. The PACES system (see section 3.2) was designed to map the shallow part of the subsurface and has been used extensively for vulnerability mapping in Denmark, but the depth of investigation for the PACES system is limited to ~25 m and the system extension limits the possible line separation to more than 100 m. The tTEM system



was designed to fill this gap in the geophysical toolbox for shallow, efficient geophysical resistivity mapping.

Scaling down a TEM-setup to make it small enough to be towed by an ATV and operating in the landscape posted several challenges. The 2x4 m tTEM transmitter loop provides a relatively small transmitter moment compared to ground based and AEM systems, hence a poorer signal to noise ratio. To overcome this, the tTEM system utilizes a very high repetition frequency, and thereby suppresses noise by more data stacking. The depth of investigation for the tTEM system well exceeds the original design goal of 50 m and a fast repetition rate ensures a high lateral resolution in the tTEM mapping results as well.

The relatively small transmitter coil makes it non-suitable to place the receiver coil in the center due to coupling between the coils and because of the presence of a strong primary EM field. Zero positioning of the receiver coil (Figure 5), as used for the SkyTEM system, was tested but found to be unfeasible. The final tTEM system therefore uses an off-set configuration to protect the receiver system from cross-coupling to the transmitter loop.



*Figure 5. Initial testing, Aarhus TEM-test site fall 2015.*



The key to obtaining very near-surface resolution is a fast turn-off of the transmitter current. Comprehensive development was carried out to obtain a fast and stable LM turn off time at  $\sim 2.5 \mu\text{s}$ .

The TEM test site has played a key role for numerous system-tests in the development phase. Since the EM-response is high at the relatively conductive test site, system tests have also been carried out on a low signal resistive site near Hvinningdal. This is needed in order to be able to detect potential small instrument bias signals. All parts of the system such as the receiver coil, the ATV, cables, GPS, etc. have been positioned after detailed testing at these test-sites to avoid bias signals based on the measurements.

The present generation of the tTEM-system is a fully tested and stable production system. At present time (end of 2019) more than 15,000 hectares (150 km<sup>2</sup>) of land has been mapped with the tTEM system primarily in Denmark, but the system has also been deployed in Tanzania, Sweden, and the U.S (Mississippi, Connecticut, Massachusetts, Pennsylvania, North and South Dakota, New York, California) and more mapping projects involving tTEM-mapping are lined up.

Further development and enhancement of the tTEM system is ongoing, at present primarily focusing on: 1) increasing the survey depth by a larger and improved receiver coil, 2) more automated data processing, 3) real time data inversion providing a real-time preliminary resistivity section with possible online streaming of the results. 4) full 3D inversion. As to point 1) a new generation of receiver coils (RC20) is already used in production, increasing the DOI with  $\sim 20\%$  compared to the older RC5 receiver coil used in the surveys presented in this report.

Development on the FloaTEM-version is also ongoing, primarily focusing on increasing the transmitter moment to be able to penetrate thicker conductive water bodies (salt water) and integration of an echo sounder for precise detection of the bathymetry to include as prior in the data inversion.

### **Technical details**

The tTEM transmitter and receiver instrumentation are built using the same technology as the SkyTEM- and WalkTEM-system, but have been heavily customized to achieve the tTEM design goals. The tTEM system transmits both a low and a high moment current pulse (LM, HM) to achieve both shallow and deep information. Key system specifications are listed in Table 1.



The current diffusion into the ground for TEM is fast, so the key to obtaining very near surface resolution with a TEM-system is a fast turn-off and immediate recording of an unbiased signal. The tTEM-system turns off the  $\sim 3$  A LM-current in  $\sim 2.5 \mu\text{s}$  and has the first unbiased time gate  $1\text{-}2\mu\text{s}$  after the current turn-off. The high moment facilitates a transmitter current of  $\sim 30$  A, with a turnoff time at  $\sim 5.0 \mu\text{s}$ . To prevent overheating in the transmitter due to the very high repetition rate and high transmitter current, the transmitter unit is water cooled.

In the modelling the of tTEM data, the shape of the waveform is described in detail, which is crucial for accurate modelling of the very early gates. As it is not possible to measure the waveform continuously, a fixed waveform, measured in detail under standard conditions is used in the modelling. To ensure a completely stable waveform the transmitter is regulated so that the temperature of the transmitting electronics is kept at  $45^\circ \pm 2^\circ$  and the current at  $30$  A ( $\pm 1$  A).

Key system parameters - tTem system, 2019		
Operating speed	15-20 km/h	
Line spacing	typical 10 - 30 m	
Effective mapping speed	$\sim 1$ km <sup>2</sup> /day (at $\sim 20$ m line spacing)	
Rx-coil	RC5, cut-off frequency of 550 kHz	
	LM	HM
Transmitter area (single turn)	8 m <sup>2</sup>	8 m <sup>2</sup>
Tx Current	$\sim 2.8$ A	$\sim 30$ A
Tx Peak moment	$\sim 22.4$ Am <sup>2</sup>	$\sim 240$ Am <sup>2</sup>
Repetition frequency	2110 Hz	660 Hz
Moment cycle: number of pulses/time	422/0.20 s	264/0.40 s
Tx on-time	200 $\mu\text{s}$	450 $\mu\text{s}$
Turn-off time	$\sim 2.5 \mu\text{s}$	$\sim 5.0 \mu\text{s}$
Gate time interval (from beginning of turn-off)	4 $\mu\text{s}$ – 33 $\mu\text{s}$	10 $\mu\text{s}$ – 900 $\mu\text{s}$
Number of gates	15	23

Table 1 Key system parameters, tTEM-system 2019.



A mapping speed of 20 km/h combined with the LM and HM pulse times listed in Table 1, results in raw data stacks per 0.6 s or each ~3.3m, holding 422 LM / 264 HM single transients. Further stacking of the raw data stack into soundings for each 10 m result in further noise suppression.

## 2.2 DATA PROCESSING AND INVERSION

### Signal pre-processing

The noise suppression techniques used in the tTEM system are similar to those used in most TEM systems. The tTEM transmitter reverses the polarity of alternating pulses and the EM response is measured in gates with an analog integrator. The gates are linearly spaced in logarithmic time to ensure sufficient time resolution in the early gates and optimum signal-to-noise at later gate times.

The raw stack sizes are chosen to cover an integer number of power line cycles to suppress power line noise. Furthermore, the pulse repetition frequencies (stated in table 1) are chosen to suppress interference from powerful VLF radio transmitters. Motion induced noise, caused by rotation of the receiver coil in Earth's magnetic field due to vibrations while driving, is efficiently suppressed by the fast repetition and advanced filtering techniques. Contrary to AEM, motion induced noise is not a major noise source for the tTEM-system.

### Data processing and inversion

The processing and inversion of the tTEM data is carried out within the Aarhus Workbench software package. Aarhus Workbench uses the AarhusInv code for modelling and inversion.

The following provides a brief description of the process, which is similar to the processing of SkyTEM data in many aspects. During data processing, couplings in data are removed, partly automatically and partly manually. Data from line turns where the ATV gets too close to the Tx-loop are removed automatically, based on the line number file that is produced while surveying. The raw data are stacked in equidistant time intervals, to create soundings with a spacing of typically ~10 m. The single data-points are assigned an uncertainty corresponding to the data standard deviation calculated from the stacking of raw transients, plus a uniform uncertainty of 2%, summarized as variances.



As for any EM-method, coupling to man-made installations e.g. power cables, gas pipes, electrical fences, etc. poses a challenge, and data coupled to these types of installations are often so heavily disturbed that they are discarded during the data processing. Compared to AEM systems and traditional single site, ground based TEM-systems, the tTEM system is much more compact, and has a significantly smaller footprint. The small tTEM footprint significantly reduces the distance to the coupling sources where undisturbed data can be obtained. For the tTEM system we can normally obtain usable data as close as 30-70 m to the coupling source, or at least twice as close as for the SkyTEM system.

The inversion of the tTEM-data is normally carried out with spatially constrained 1D smooth models (SCI), forming pseudo 3D model spaces. The inversion algorithm includes modelling of all the key parameters of the system transfer function, such as transmitter waveform, transmitter/receiver timing, low-pass filters, gate widths, and system geometry, which are all essential in order to obtain accurate data modelling and provide minimally biased inversion results. The inversion result is accompanied by an estimate of depth of investigation (DOI). The regularization scheme/model type can be either *blocky* (L1-norm), *smooth* (L2-norm) or *sharp* (minimum support norm), hence the inversion setup can be customized according to the geological setting.

For the test-site tTEM-dataset used for validation in chapter 4, a laterally constrained inversion setup (LCI) has been used, while the field cases in chapter 6, uses the SCI setup. Both the smooth and the sharp regularization schemes are used for the tTEM test site dataset and in the synthetic modelling study, which includes ERT and PACES as well.



### 3 METHODS – PACES AND ERT

In the modelling resolution study and for field case examples we are comparing the tTEM system with the PACES system and ERT. Section 3.1 and 3.2 therefore, holds a short description of the PACES and ERT method, while some of the basic differences in the physics between tTEM and ERT/PACES are discussed in section 3.3.

#### 3.1 ERT

DC resistivity, multi-electrode systems often called ERT: Electrical Resistivity tomography (ERT), CVES: Continuous Vertical Electrical Sounding (CVES), or in Denmark MEP: Multi Electrode Profiling, have frequently been used for geophysical mapping in Denmark.

With the ERT, a current is injected into the ground using two electrodes and the resulting voltage is measured over other two electrodes. The voltages are indicative of the subsurface resistivity. A multi-electrode system consists of electrodes, typically 50 – 100, placed along a profile line with a uniform distance of typically 2-10 m. Each electrode is connected to the transmitter-receiver instruments using multi-core cables. The instrument switches between a large number of quadruple configurations, thereby obtaining 2D data coverage. Line oriented ERT data are normally inverted to 2D resistivity sections.

In Denmark, in a groundwater mapping context, ERT has most often been configured with an electrode spacing of 5 m and with a 400 m electrode layout. To obtain transects longer than 400 m, the roll-along technique is applied, where the first 100 m of cable is “rolled” to the other end of line and a new measurement is made. Older ERT measurements are normally carried



*Figure 6. ERT.  
Electrodes and cables*



out using Wenner and Schlumberger like configurations, while newer ERT profiles, recorded with a modern multi-channel ERT system, most often uses Gradient Array configurations. With a 400 m layout and an electrode spacing of 5 m, the depth of investigation is typically 70-100 m, thus similar to the tTEM-system. The mapping speed is relatively slow. With the above described ERT-setup, 2-3 people can conduct 1-2 km profile per day. Despite the relatively slow mapping speed, ERT has been used for area mapping in Denmark, especially on Zealand, by making multiple transects with a line spacing of typically 300-500 m.

### 3.2 PACES

The Pulled Array Continuous Electrical Sounding system (PACES) (Sørensen, 1996) is a DC-method that records data from eight quadrupole configurations continuously, while pulling a ~100 m long electrode tail on the surface (see Figure 7 and Figure 8). The operation speed is ~6-7 km/h, and the system provides detailed resistivity information down to a depth of 20-25 m. The spatial resolution is achieved with a line spacing of typically ~300 m and a resistivity model spacing of 10 m along the lines. Due to the relatively long turning radius, the PACES surveys were typically carried out as relatively long survey lines across several fields.

PACES data were inverted with a 1D three layer model in a laterally constrained inversion setup (Auken et al., 2005). With eight data points per model a three layer model is the most that can be supported. Multi-layer models (smooth models) with vertical constraints between layers would also be an option, but the 3-layered model has been the preferable one for most PACES data collected in Denmark.



Figure 7.  
PACES electrode tail.



During the 1990s, the PACES system was used widely in Denmark, primarily for vulnerability mapping, and the national geophysical database (GERDA) holds approximately 10,000 line km PACES data covering approximately 3000 km<sup>2</sup>.

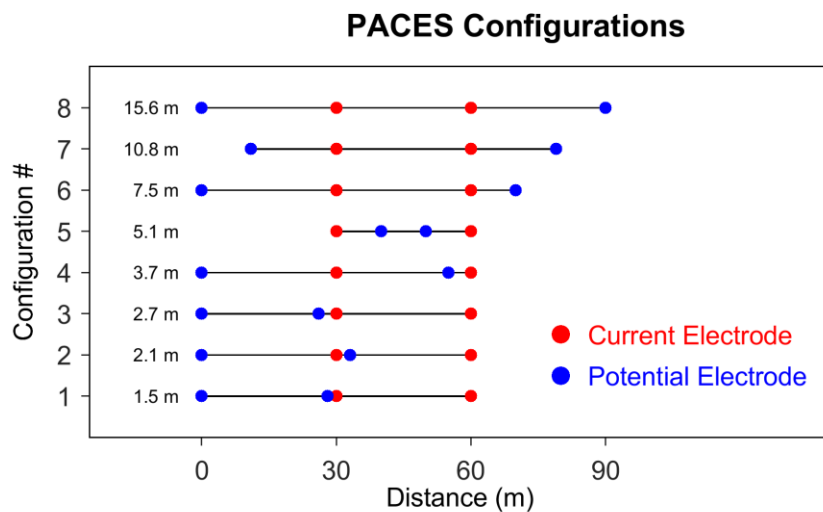


Figure 8. The eight PACES configurations. The numbers to the left are the focus depth (the depth were you reach 50% of the total sensitivity for the configuration on a half space, 1D-model).

### 3.3 RESOLUTION AND MAPPING CAPABILITY

Both PACES, ERT, and tTEM, map the electrical resistivity of the subsurface. While PACES and ERT are DC-methods that inject an electrical current directly in the ground using electrodes, tTEM is an EM-method, which induces electrical currents in the ground through the principle of electromagnetic induction. The physics behind the DC- and the EM-methods are quite different, which has an impact on resolution, foot print size, and model equivalences. This should be taken into account in the different comparison examples.



### Anisotropy

As shown in Figure 9, the current runs both horizontally and vertically in the ground for a DC measurement. The obtained layer resistivity for DC-methods ( $\rho_{DC}$ ) is therefore influenced by both the vertical and horizontal resistivity of the layer, as given by:

$$\rho_{DC} = \sqrt{\rho_V \cdot \rho_H}$$

where  $\rho_V$  is the resistivity in the vertical direction and  $\rho_H$  is the resistivity in the horizontal direction of a layer. For tTEM the current only flows in the horizontal plane (Figure 9), which means that the layer resistivity retrieved with tTEM corresponds to the horizontal resistivity ( $\rho_H$ ). Thus, if the resistivity in the two directions within a layer is different, i.e. the layer is anisotropic, the obtained layer resistivity for the DC-methods will be different from that obtained with the tTEM-method.

For example, anisotropy occurs when a layer internally contains thin conductive clay layers (macro anisotropy), which causes the horizontal resistivity to be smaller than the vertical. In such cases, a DC method with a 1D model will over-estimate layer thicknesses and the tTEM method will provide a lower layer resistivity than the DC method. Anisotropy can also occur as a result of specific clay minerals lattice structures (micro anisotropy).

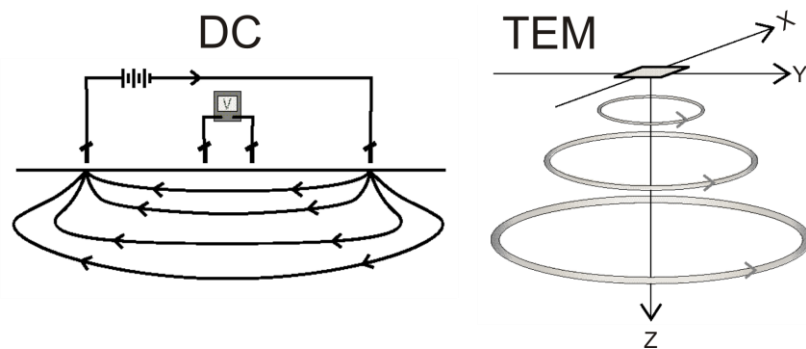


Figure 9. Principle sketches of the current flow in the ground. Left: DC setup with surface electrodes. Right: TEM setup with a horizontal transmitter loop.



### **Model equivalences and resolution**

Model equivalence is when several resistivity models explain the recorded within the data uncertainty, and is primarily an expression of the physical resolution limitation of a method. For both the TEM and DC method, the ability to resolve a layer depends on the resistivity contrast to neighboring layers and the thickness of the layer, but the sensitivity and responses scale differently.

The data response from a DC-method scales relatively with the layer thickness and resistivity, thus the DC-method resolves a resistivity contrast of 1-10  $\Omega\text{m}$  equally well as a contrast of 100-1000  $\Omega\text{m}$ . Equivalence problems are relatively pronounced for the DC method. The high- and low-resistivity equivalences imply that only the product, or the ratio, of the resistivity and layer thickness can be resolved for the equivalent layers. This means that the layer thickness and boundaries for the equivalent layer are poorly determined, and with possible over or under estimation of the true resistivity.

In contrast to the DC method, the TEM method is sensitive to absolute contrasts in the conductivity domain (conductivity =  $1/\text{resistivity}$ ). This makes the method good at resolving layer sequences involving conductive layers, and less good at resolving layer sequences only involving very resistive layers. High and low resistance equivalence does not display to the same degree for the TEM method.

For both the TEM and DC methods, the resolving capability decreases with depth, meaning that the layer thicknesses and/or the resistivity/conductivity contrast must increase with depth, in order for a layer to manifest itself in the data, and thus in the obtained resistivity model.

### **Footprint and resolution**

Of course, the data sampling density has a big influence on the lateral resolution, although a single DC or TEM measurement does not provide point information, but samples a larger volume of the subsurface – the footprint.

The footprint of a DC measurement corresponds approximately to the distance between the electrodes and is very focused in the profile direction. For ERT and PACES, the short configurations sample the near surface while the longer electrode configurations sample the deeper parts. In other words, the foot print increases and the lateral resolution decreases with depths.

For the TEM method, the circular current system diffuses downward and outward, so as with the DC-methods the foot print increases with depth. For



a central loop TEM system the footprint is circular, and for a TEM sounding the radius of the footprint is approximately twice the depth (1D half space case). The tTEM system uses an off-set configuration, but except for the very shallow part, the footprint is near-circular. Hence, the footprint of the tTEM system is much wider perpendicularly to the survey lines than in the ERT/PACES case. The minimum tTEM footprint size for the very shallow part corresponded approximately to the size system layout of ~12m.

### **Depth of investigation – DOI**

The sensitivity decreases with depth as mentioned. How deep a given geophysical method can identify structures is a matter of how much sensitivity is needed to have trust in the results. The modelling and inversion code AarhusInv estimates the depth of investigation (DOI) for each resistivity model, based on a sensitivity threshold value. The estimated DOI value takes the following into account:

- The geophysical method and system setup ie. *the system transfer function*
- The number of data points
- The data uncertainty of each data point
- The current resistivity model

The DOI presented on the various sections in this report is based on the DOI-standard threshold value, as also used in the Aarhus Workbench software. As a guideline, resistivity structures below the DOI-standard value are based very weakly in the data. The DOI estimate does not take the enhanced resolution from lateral constraints into account.

## **3.4 ACCUMULATED CLAY THICKNESS**

Together with boreholes and geochemical information, PACES mapping results have been a main source of information for groundwater vulnerability assessments in Denmark. In a vulnerability mapping context, the PACES resistivity results have often been used to estimate the accumulated clay thickness in the upper 30 m (referred to as ACT). In the later modelling study and for the field examples, we will also compare the ACT calculations for the different methods.



For a layered resistivity model, the ACT in a depth interval is then calculated as:

$$\text{ACT} = \sum_{i=1}^N W(\rho_i) \cdot t_i$$

where  $N$  is the number of layers in the calculation interval,  $W(\rho_i)$  is the weight from the translator function showed in Figure 10, for the resistivity in layer  $i$ , and  $t_i$  is the thickness of the layer. The translator function (Figure 10), basically informs when a resistivity value should be interpreted as clay (<50  $\Omega\text{m}$ , weight=1), or as non-clay (>70  $\Omega\text{m}$ , weight=0), with a transition zone (50-70  $\Omega\text{m}$ ), where a resistivity value is interpreted as partly clay and therefore is assigned a weight between 0-1. The translator function can either be fixed for an entire survey or be changed spatially based on lithological borehole information using the ACT modelling concept. Typical *upper* and *lower* threshold values for the translator model in Denmark are 70 and 50  $\Omega\text{m}$ .

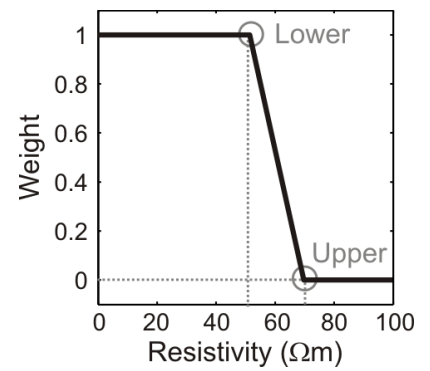


Figure 10. ACT translator function, defined by a lower and an upper threshold value.



## 4 TTEM TEST-SITE VALIDATION

In this section, we show the results of a detailed validation of the tTEM system, in both model space and data space, based on multiple runs at the east-west reference line at TEM test site. The validation examines both the repeatability for the tTEM-system and the match to the test site reference section. A similar validation study of the SkyTEM system can be found in the GFS-report "*Validation of the SkyTEM system at the extended TEM test site*" (see the reference list)

### 4.1 TEM TEST SITE

The Danish TEM test site at Aarhus was established in 2001, with the aim of getting the nine different ground-based Geonics TEM47/PROTEM systems operating in the Danish groundwater mapping campaign to produce the same TEM responses at a given point location, which was far from the case initially. After instrument repairs, updates, and minor time and data shifts, it was possible to get the nine TEM systems to produce consistent TEM responses with a deviation within roughly 3% for the low-noise part of the sounding curve. Based on these nine responses, an average response was calculated and appointed as the reference response for the test site. For validation and calibration of other TEM-systems, the reference response was inverted to a 5-layer resistivity model, and this model was appointed to be the TEM reference model for the site. In 2011, the upper ~15 m of the reference model was refined based on shallow electrical resistivity tomography (ERT) measurements and a detailed electrical conductivity log.

In 2011, the TEM test site was extended to include two orthogonal lines approximately one kilometer long (reference lines). This extension was primarily carried out in order to be able to validate AEM systems under production conditions and to enable calibration of AEM systems that cannot make hovering measurements. The reference lines were carried out with a pre-calibrated WalkTEM system in a central loop configuration with a 40x40m<sup>2</sup> transmitter loop. The square in Figure 2 marks the positions of the reference line models for the east-west reference line, which is the line used to validate the tTEM system. Note that the upper ~15 m refinement was only carried out for the point reference model (the red square in Figure 2).

Detailed information regarding the Aarhus TEM test site and calibration/validation of TEM-system can be found in the paper "*Test site calibration and validation of airborne and ground based TEM systems*" (see the reference list).

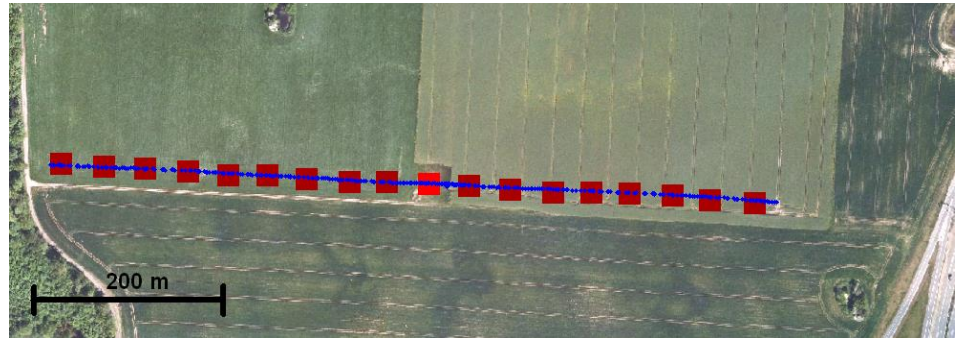


Figure 11. The East-West TEM reference line at Aarhus TEM test-site. Blue dots mark the data/model position of the four tTEM repetitions. The squares mark the positions of reference models. The red squares mark the point reference location.

## 4.2 THE TEST SITE DATASET

### System setup and calibration

The tTEM dataset for validation from the test site was carried out on September 18, 2019, with the instrument set TX03-Tib18-RC20. Standard production setup and measuring script (as described in section 2) was used for recording the data along the east-west reference line. Four line repetitions were carried out, two in each direction, with a normal production speed of approximately 20 km/h. The tracks of the four repetitions are shown with blue dots in Figure 2. Position wise, the four repetitions coincide very accurately and they coincide with the center of the reference line soundings/models.

Prior to the data collection, the tTEM system was calibrated at the point reference spot following the standard calibration procedure. Figure 12 shows the low and high moment calibration plots and the obtained calibration parameters, which are all within the normal ranges.

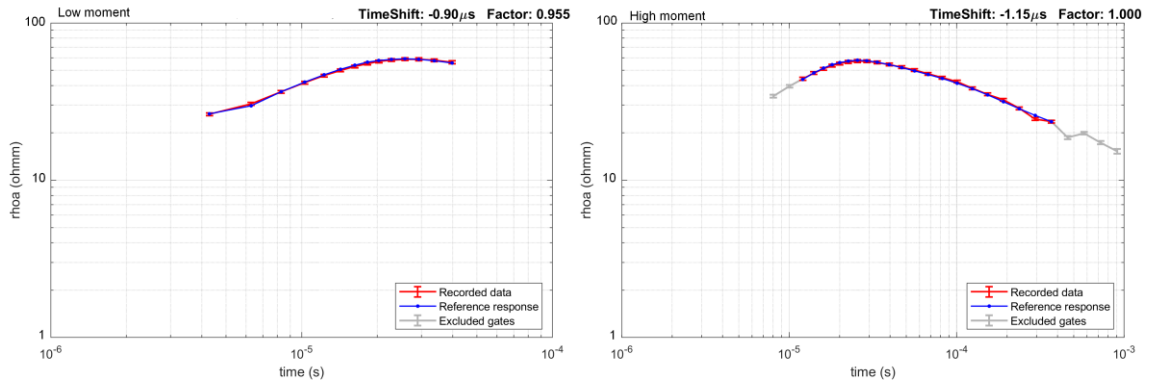


Figure 12. *t*TEM low moment (left) and high moment (right) calibration plots. The blue curve is the reference response while the red curve/red error bars are the recorded data after calibration. The obtained calibration time-shifts and factor-shifts are stated at the top of the plots.

### Processing and inversion

Data processing and inversion were carried out in the Aarhus Workbench software, utilizing the AarhusInv code for inversion in the standard approach. The processed data were sampled to soundings at even time-steps resulting in approximately one sounding per 10 m. Figure 13 shows the high moment data section for one of the repetitions of the reference line. As observed in the raw data section, we encountered some noise bursts. Noise bursts of these kinds are normally rarely observed in the *t*TEM data, and we have not been able to determine the source of these noise bursts. As seen in the stacked data section in Figure 13, the noise bursts partly stack out, but in some cases it has been necessary to increase the data uncertainty or delete the affected data points. The noise bursts are not observed in the low moment part, probably due to a much higher  $db/dt$ -signal. The noise bursts do not influence the validation significantly, but result in an uneven number of data points per sounding along the reference line, and hence a more uneven DOI throughout the reference line.

The data uncertainty arises from the data stacking plus a uniform 3% uncertainty. For the two first low moment gates, the uniform uncertainty is increased to 5%, since the time gate very close to the instrument front gate is very sensitive to even tiny inaccuracies in the waveform description, front gate timing, etc.



The data stacking was performed with a 2 s running mean box filter for the low moment and a running mean box filter with an increasing width from 2 s up to 10 s for the very late time gates for the high moment.

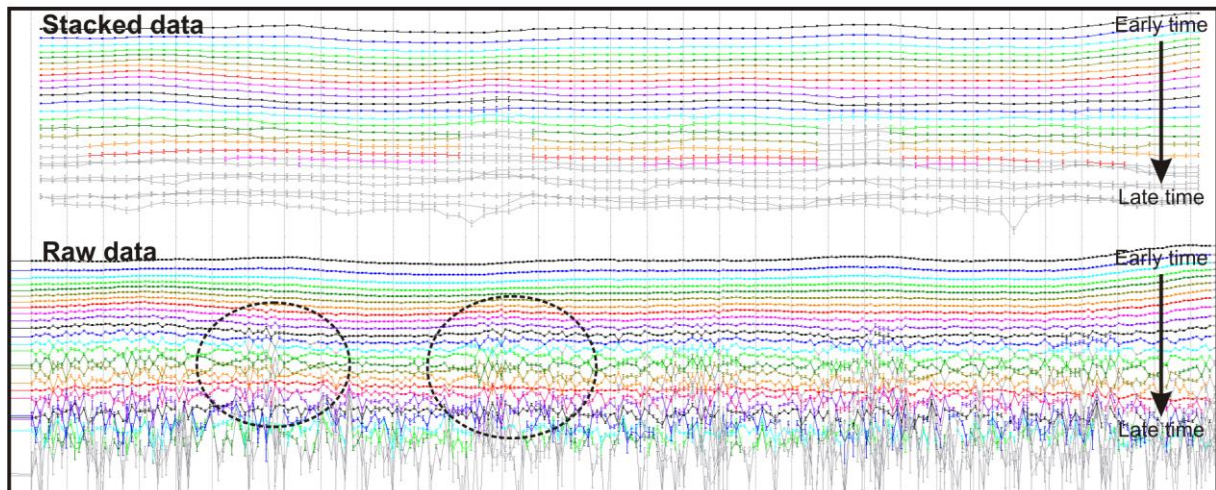


Figure 13. High moment data section from the reference line, ~700m (repetitions 3). The top section shows the stacked data that enter the inversion. The bottom section shows the raw data. The dashed circles outline some of the noise bursts observed in the data. Gray data points indicate disabled data that do not enter the stacking/inversion.

The processed tTEM data were inverted with the standard LCI approach, which includes modelling of the transmitter and receiver geometry, transmitter waveform, low-pass filters etc. The line repetitions were inverted in separate LCI sections, with both a 4-layer model, and with the smooth and sharp model regularization schemes. The smooth and sharp models used a 30 layer model with logarithmically increasing thicknesses from 1m to ~8m down to a depth of 100 m, while the 4-layer model includes both layer thicknesses and layer resistivities as inversion parameters. All inversions were started from a 50  $\Omega$ m half space. Standard LCI constraints/regularizations were applied.

The normalized data fit with respect to the data uncertainties are similar for the different inversion types and line repetitions, and are all well below 1, meaning that the data fit well within the estimated data error.



### 4.3 VALIDATION MODEL SPACE

The first validation step of the tTEM system at the TEM test site is a simple visual comparison of the inversion results of the four repetitions, which for the smooth model inversions are shown in Figure 14. Inversion results for the different inversion types and for all repetitions are included in Appendix 1 .

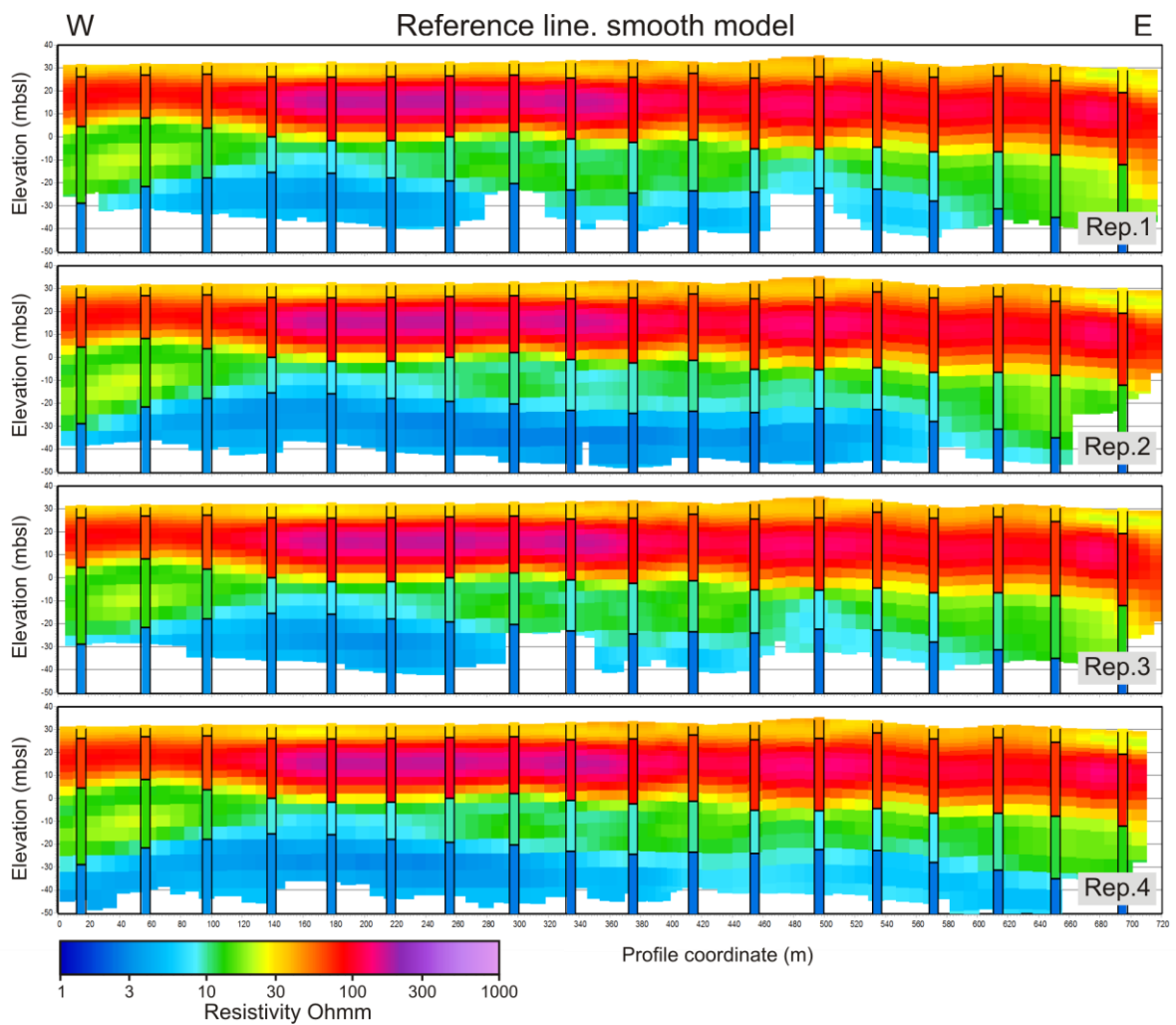


Figure 14. The four tTEM repetitions of the reference line. Smooth inversion results, blanked at the DOI.



As seen in Figure 14, the four sections are very similar and no effect of the data recoding directions is observed (repetitions 2 and 4 are recoded in opposite direction of 1 and 3). The minor dissimilarities are mainly observed in the DOI, caused by the uneven number of late time, high moment data points, and in the deeper conductive model part, which is likely a consequence of model equivalence. In general, the agreement between the sections is excellent, and from a geological interpretation point of view, the sections are identical.

Figure 15 shows a comparison of the reference line models with both a smooth, a 4-layered, and a sharp tTEM inversion for three different line repetitions. The most straight-forward comparison is the four-layered tTEM section with the layered reference models (Rep. 2, 4-layer in Figure 15), since they are both based on a *layered* inversion. The match to the reference line for Rep. 2, 4-layer in Figure 15 is very good and both the layer boundaries and the resistivities match very well. Even the lateral resistivity variations in the 3<sup>rd</sup> layer are relatively consistent in the two results. The tTEM slightly offsets the first layer boundary by a few meters compared to the reference models, which is also the case for the other sections in Figure 15. This minor offset can be explained by the fact that the tTEM-system has both a smaller footprint and a better near surface resolution (earlier time gates) than the WalkTEM soundings that the reference models are based on, or that we are looking at equivalent models.

The comparison of the reference models to the smooth and sharp tTEM inversion results in Figure 15 is more fuzzy because of the different model setups and regularization schemes. As for the 4-layered section, an overall good match is observed, with a slightly over-estimation of the thickness of layer two.

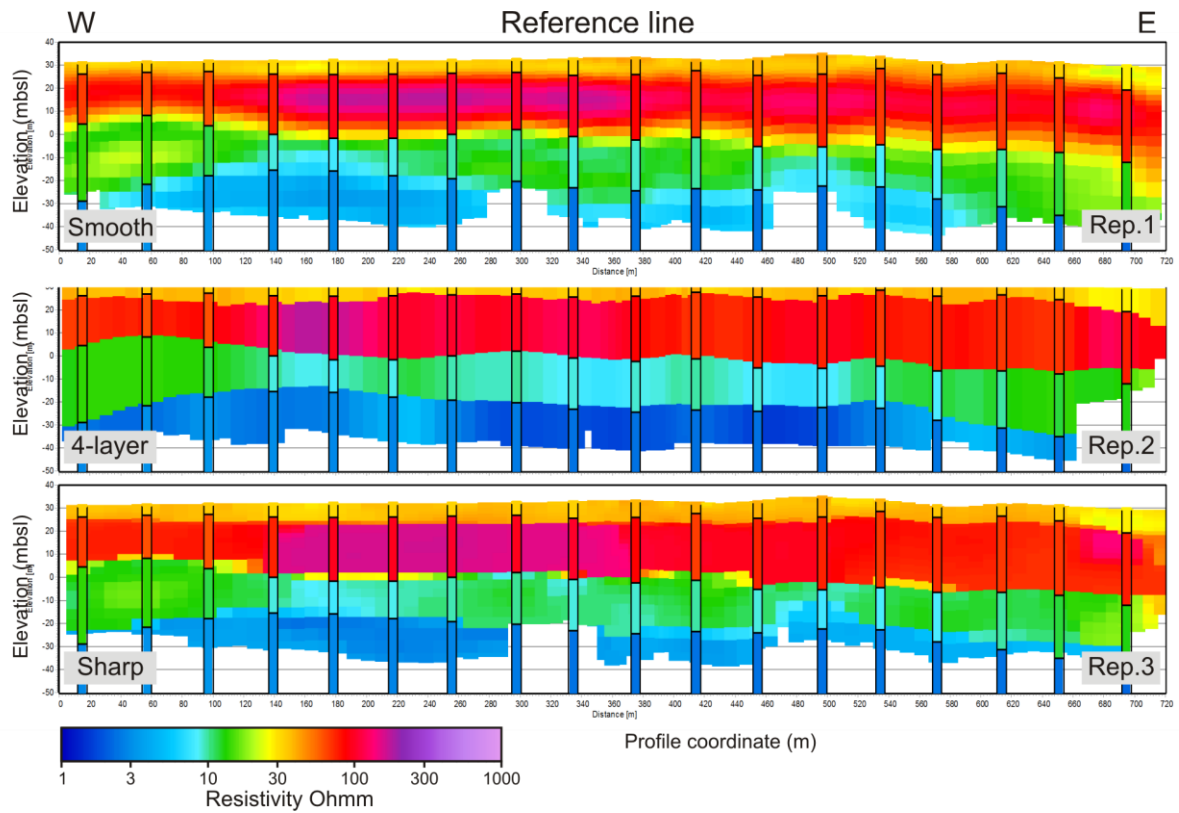


Figure 15. Comparison with the reference models for three different repetitions and inversion types. The background sections are the *t*TEM results while the front bars are the reference models. Rep.1) Smooth inversion of the 1<sup>st</sup> line repetition. Rep. 2) 4-layer inversion of the 2<sup>nd</sup> line repetition. Rep. 3) Sharp inversion of the 3<sup>rd</sup> line repetition.



In general, the tTEM results reproduced the reference line models very well and well within our expectations, taking into account that we are comparing to another TEM-method with a different footprint and resolution.

#### 4.4 VALIDATION DATA SPACE

In this section, we perform a detailed validation of the tTEM system by comparing in data space instead of comparing inversion results as above. By making the comparison in data space, we take the model equivalence issues out of the equation, and the repeatability and the match to the reference can be evaluated for the individual gate times.

The repeatability test will be done by comparing the recorded data from the four line repetitions gate by gate. To be able to validate the recorded data against the reference, we first need to calculate a tTEM 1D-forward response for the reference models with exactly the same system specification as for the tTEM-system used at the test site. This tTEM 1D-forward response is referred to as the reference response in the following.

In Figure 17 the recorded data for three LM and four HM gates (the error bars) are plotted. Each color of the error bars represents a line repetition. The selected LM and HM gates plotted in Figure 17 are marked on a single sounding curve in Figure 16. Appendix 2 holds plots like Figure 17 for all the LM and HM time gates. The size of the error bars for relatively noise free gates (panel 1-5, Figure 17) are approximately equal to the uniform uncertainty of 3% (5% for LM gate 1, see section 2.2) while the error bars increase for the later time gates (panel 6-7, Figure 17), since we getting closer to the background level. The red dots in Figure 17 are the reference responses, to which we will come back.

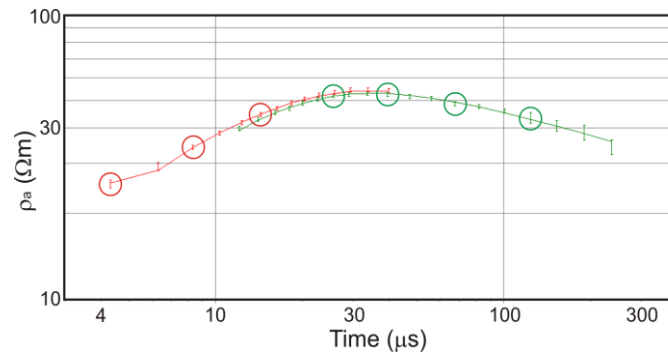


Figure 16. A single tTEM sounding with low moment part in red and high moment part in green. The red and green circles mark the gate times that are plotted for the full reference line length in Figure 17.

### Repeatability

Based on the data plots in Figure 17 of the four tTEM repetitions, we can observe and conclude the following with respect to data repeatability:

- In general, the tTEM data repetitions are very good and within the data uncertainty.
- For the relatively noise free gates in Figure 17 (panel 1-5) the repeatability is perfect - one can hardly distinguish between the different colored error bars from the four line repetitions.
- The first LM gate at  $\sim 4.3 \mu\text{s}$  (panel 1, Figure 17) has a jagged appearance. However, they coincide in the four repetitions, which means that they cannot be noise spikes or instrument instability. This gate is very close (in time) to the current turn-off and the protective front gate in the instrument, which means that it is very sensitive to even small resistivity variations in the top soil, resulting in the jagged appearance.
- For the late time HM gates 13 and 16 (panel 6-7, Figure 17) the signal is closer to the background noise level and the data have larger uncertainty/error bars, but the repeatability is still quite good and within the data uncertainty.
- The relatively uneven sizes of the late time HM error bars are primarily a result of the noise bursts mentioned above that are present in the dataset.

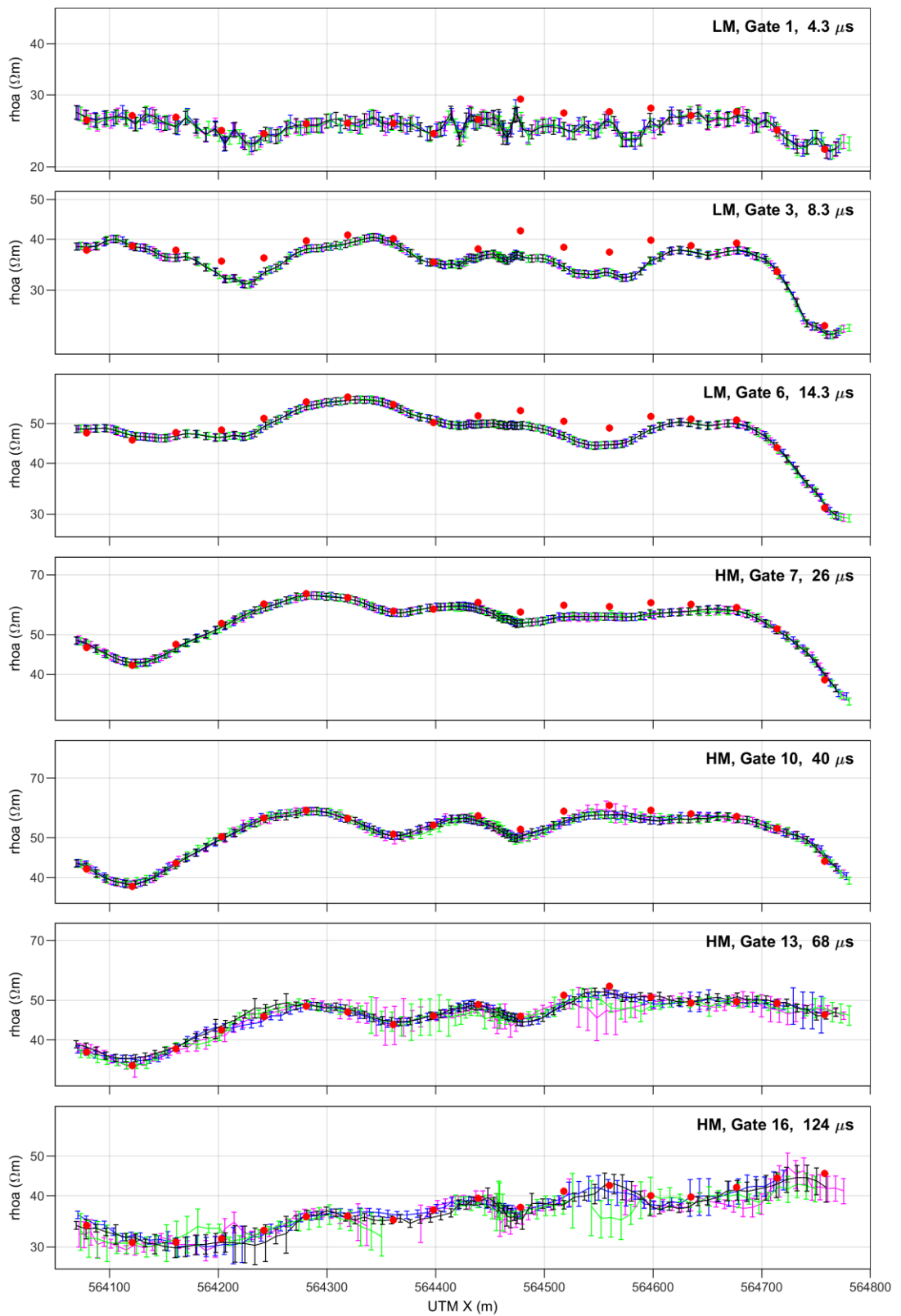


Figure 17. Data plot of LM and HM time gates from the reference line. The error bars mark the recorded  $t$ TEM data. Each color represents a line repetition. Red dots mark the reference response.



### **Validation to reference response**

Focusing on the match to the reference response (the red dots in Figure 17) we observed the following:

- The overall lateral data variations are very similar in the tTEM-data, and the match to the reference response is reasonably good.
- The match to the reference response is better for the later/deeper time gates.
- No systematic offset/errors are observed.
- In a part of the section (~564450-564600 m), the tTEM LM gates (panel 1-3) display a minor mismatch to the reference response of approximately 2 times the size of the error bar.

It is expected that a potential mismatch to the reference response would be most likely to occur for the very early time gates, where footprint and resolution differences between the reference TEM-system and the tTEM-system are largest. Though the mismatches are isolated to a few gates and only at some parts of the line. We do not observe systematic errors such as a single gate time being consistently shifted, or a general offset of the tTEM data with respect to reference. Any of these mismatches would have been a clear indication of some sort of system error. For the later time gates, we obtain a fine match within the data uncertainties. Overall, we obtain a good match to the reference response for the tTEM-system.



## 5 MODEL RESOLUTION STUDY - TTEM, PACES, ERT

In the model resolution study and in the later field case examples, we compare the tTEM system with the PACES-system and an ERT system. The modelling scheme is described in section 5.1, with results and discussion in section 5.2.

### 5.1 THE MODELLING SCHEME

The model resolution study shows us how well the PACES, ERT, and tTEM resolve different layered resistivity models, and since the true model is known, the evaluation is relatively straight forward. The focus is on the vertical resolution and layer recovery, primarily in the upper ~40m. The modelling is performed with a 1D setup and does not examine the methods' different lateral resolution capabilities or ability to resolve 2D or 3D structures, nor are we simulating a constrained inversion setup.

The modelling scheme consists of the following steps:

1. Calculate a method-specific 1D forward response for the true layered model.
2. Estimate realistic data uncertainties for the different methods.
3. Perform a 1D inversion of the data including DOI estimates.
4. Compare the inversion results from the different methods and evaluate the results against the true model.
5. Calculate ACT values in the depth interval 0-25 m with a fixed translator function, for the true model and for the inversion results of the different methods.

For tTEM and PACES, we model the systems as described previously. For ERT we simulate a 5 m electrode spacing in a gradient array layout. Since our modelling is 1D we have constructed an ERT sounding that includes all the unique gradient configuration of a 400 m long electrode layout. This ERT sounding contains 24 unique gradient configurations as shown in Figure 18. Selecting all the unique configurations in this way adds slightly more weight to the deeper model parts than the usual 2D layout, since a 400 m 2D layout only holds a few data points for the deepest/longest configurations, while all configurations are always present in this 1D approach. Additional modelling setup parameters are listed in Table 2. Appendix 2 holds



the exact setup files for the different methods used with the modelling code AarhusInv.

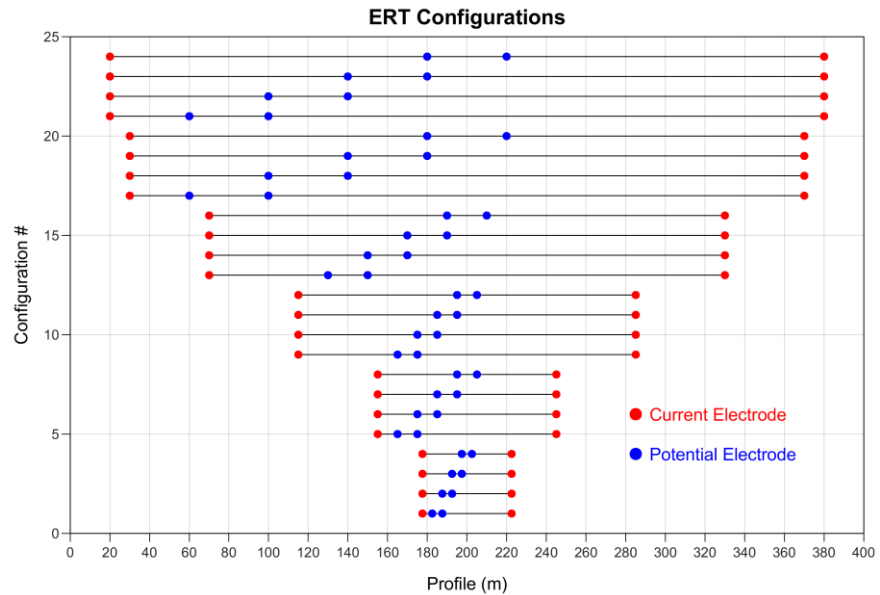


Figure 18. The 24 ERT gradient array configurations used for the 1D ERT sounding. The mirror-configurations (left/right versions of the same electrode combinations) are not included in the 1D sounding since they do not contain new information.

	<b>tTEM</b>	<b>PACES</b>	<b>ERT</b>
<b>Configuration</b>	As described in section 2	8 quadrupoles, dipole and Wenner types	24 gradient-array quadrupole configurations. Min. electrode spacing 5 m
<b>Data uncertainty</b>	Model dependent, based on a noise level at 0.8nV/m <sup>2</sup> at 1 ms plus a uniform contribution of 3%. Data points removed if STD >30%	Uniform 5%	Uniform 5%
<b>Inversion setup</b>	Model type: Smooth 1D-model Thickness first layer: 1 m Depth to last layer: 100 m Start resistivity: Homogenous half-space (no structure in the start model) Vertical constraints factor: 2 Lateral constraint factor: None		
<b>ACT</b>	Interval: 0-25m Translator function: Fixed, Upper=70 Ωm, lower=50 Ωm		

Table 2. Additional modelling parameters.



To span different model/resistivity scenarios we have created a number of model sweeps, like panel a) in Figure 19. In each model sweep, we vary one model parameter (layer thickness or resistivity) throughout the sweep.

## 5.2 MODELLING RESULTS AND DISCUSSION

Four model sweeps are presented and discussed in this section. Appendix 4 holds additional model sweeps without any further comments.

Figure 19 holds the first model sweep to examine. The model plot a) in Figure 19 is a four-layer model with an alternating resistivity layering of: 200, 40, 100, and 40  $\Omega\text{m}$ . The thickness of layer one increases through the model sweep from 1 m to 25 m corresponding to the model number, while the thicknesses of layers two and three are constant at 10 m and 30 m respectively. Smooth PACES, ERT, and tTEM inversions of the model sweep are shown in Figure 19b-d.

The key observations for model sweep A in Figure 19 are:

### 1<sup>st</sup> layer

- Layer one is well resolved throughout the model sweep for PACES and for ERT except for the 1 m case.
- For tTEM we observe the resistive top layer when it is 2-3 m thick, while a thickness of ~7m is needed to get a resistivity value close to the true resistivity.

### 2<sup>nd</sup> layer

- The conductive second layer is well resolved throughout the model sweep for tTEM.
- ERT has a good resolution of the layer when it is located in the upper 15-25 m, but with an increasingly poorer resolution with depth, resulting in an increasing diffuse appearance throughout the model sweep and an increasing over-estimation of the layer thickness and under estimation of the layer resistivity.
- PACES recovers the conductive second layer well until we get close to a DOI of ~24m.
- It is the conductive second layer in the true model that contributes to the ACT-value and how well the true ATC-values are recovered corresponding to how well the different methods resolve this layer, resulting in the best ACT estimates from the tTEM method.

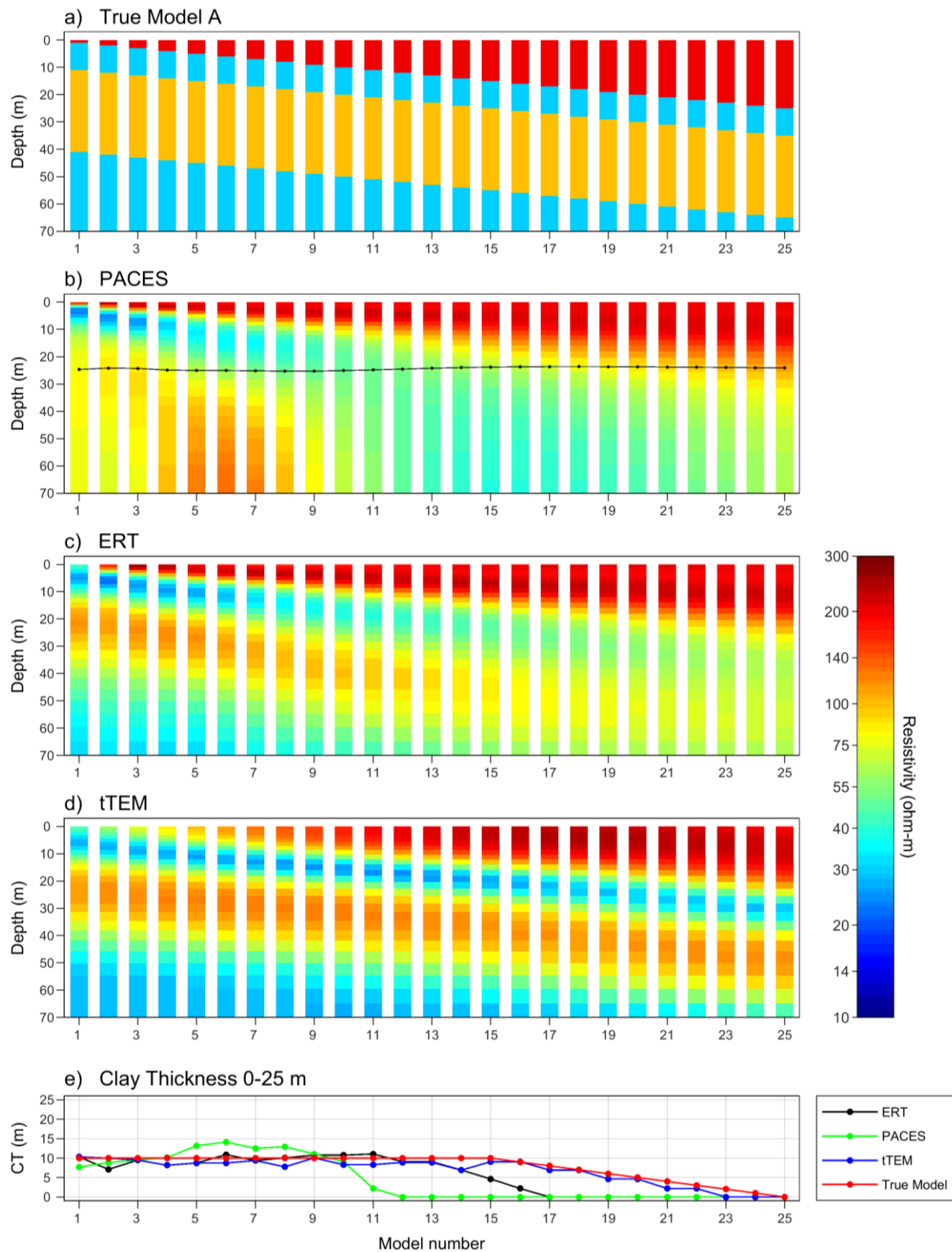


Figure 19. a) True model (200, 40, 100, 40  $\Omega\text{m}$ ). b) PACES, c) ERT, d) tTEM inversions. Black lines indicate DOI. DOI for ERT and tTEM plots deeper than 70 m. e) Clay thickness 0-25 m.



### 3<sup>rd</sup> layer

- The third resistive layer and the boundary to the bottom conductive layer are well resolved for the entire model sweep in the tTEM case.
- ERT delivers a fine layer recovery in the first 1/3 of the model sweep, but with an increasing diffuse layer appearance for the last 2/3 of the model setup.
- In the PACES case, the resistive-conductive layer sequence is not resolved at all since it is well below the DOI.

For the model sweep in Figure 20, we again have a four-layer alternating resistivity model, but this time we changed the thickness of the resistive second layer, again from 1 to 25 m, while the conductive first and third layers are fixed at 10 m and 30 m respectively. Like in the first model sweep, smooth PACES, ERT, and tTEM inversions are shown in Figure 20.b-d. The key observations for the model sweep B in Figure 20 are:

### PACES

- PACES resolves the first layer and the layer boundary to the second layer well when the thickness of the second layer is >5m.
- The deeper part of the model cannot be resolved by PACES, either because it is below the DOI or the second layer is too thin.

### ERT

- The ERT resolves the model sweep relatively well.
- When the second layer gets thin, we get an overestimation of the layer thickness and an underestimation of the resistivity.
- The depth to the last layer is poorly resolved in most of the model sweep.

### tTEM

- The tTEM does a similarly good job of resolving the model sweep as the ERT.
- The second layer needs to be a few meters thicker to be resolved as well as in the ERT case.
- The tTEM resolves the conductive third layer better than the ERT, and thereby resolves layer boundaries better than the ERT.

### ACT

- Overall, tTEM provides the best ACT-estimates
- ERT and PACES significantly underestimates the ACT, when the resistivity of the second layer is thin (1-7m), due to an overestimation of this layer thickness.

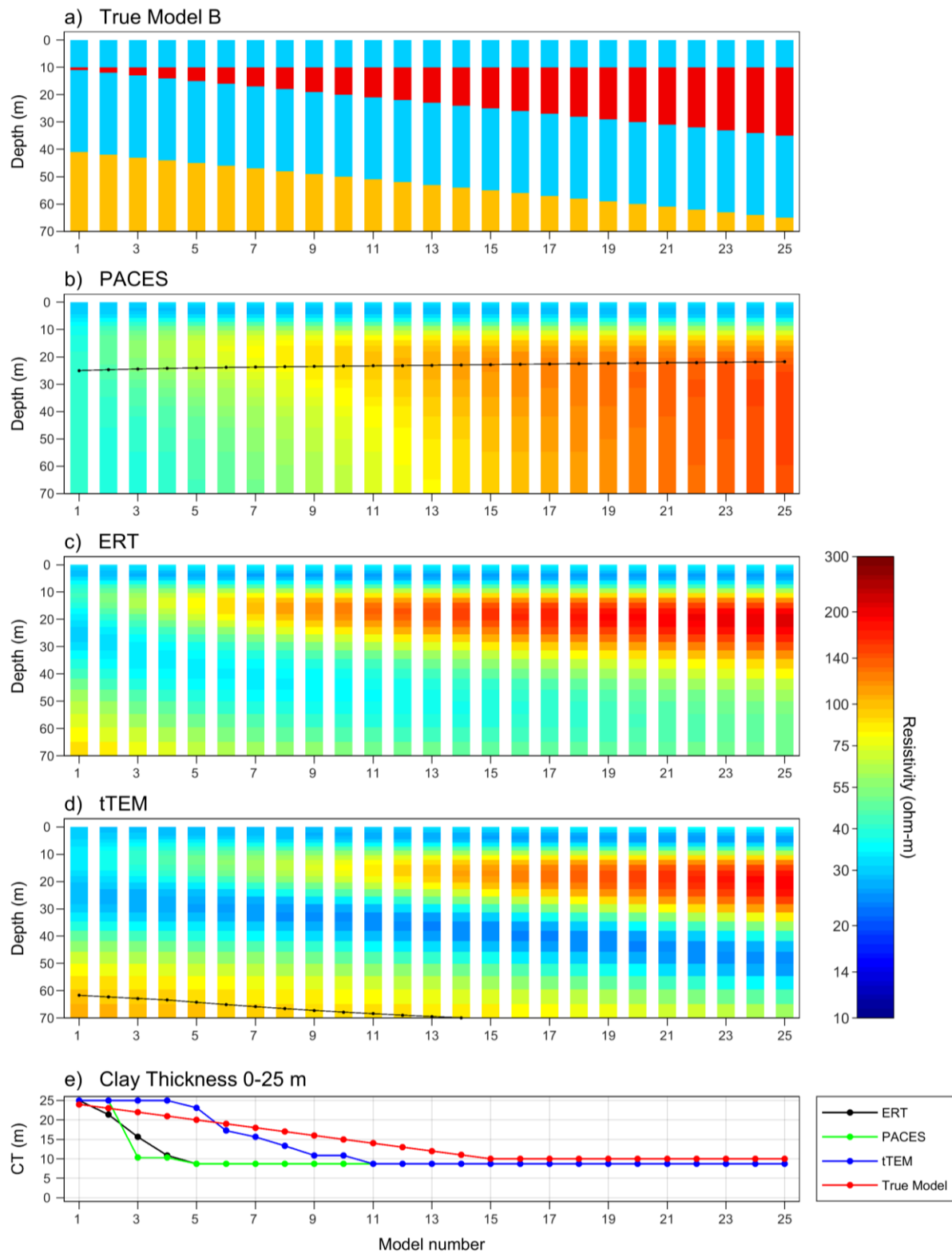


Figure 20 a) True model (40, 200, 40, 100  $\Omega$ m). b) PACES, c) ERT, d) tTEM inversions. Black lines indicate DOI. DOI for ERT plots deeper than 70 m. e) Clay thickness 0-25 m.



In the two next model sweeps, C and D (Figure 21, Figure 22) we change the resistivity of a 5 m thin layer, sandwiched between conductive layers and resistive layers respectively. Hereby we can examine how well the different methods resolve relatively thin layers with respect to the resistivity contrast. The two model sweeps are relatively challenging since they contain two 5 m thin top layers. The resistivity of the second layer is changed logarithmically from 5 to 500  $\Omega\text{m}$ .

The key observations to be made from Figure 21, where layer two is placed in a conductive sandwich of 40  $\Omega\text{m}$ , are:

- The resolution of the model part above the PACES DOI line is very similar for the two DC-methods, PACES and ERT.
- PACES and ERT overestimate the thickness of layer two in the conductive and resistive ends, partly caused by model equivalence issues for the DC-method, and partly caused by a large resistivity contrast to the surroundings layers, which results in a longer vertical transition zone in the smooth models.
- The tTEM does a better job of estimating the thickness of layer two than the DC-methods when it is conductive, but has difficulty with resolving the layer when it is resistive.
- The deeper part of the model is slightly better resolved with tTEM than ERT.
- Again, tTEM provides the most correct ACT estimates, but only slightly better than ERT.
- All three methods, but most significantly PACES, underestimate the ACT when the second layer is resistive, due to a poor resolution of this layer.
- ERT and tTEM provide similar ACT estimates, while PACES provides poor ACT estimates when the second layer is very conductive.

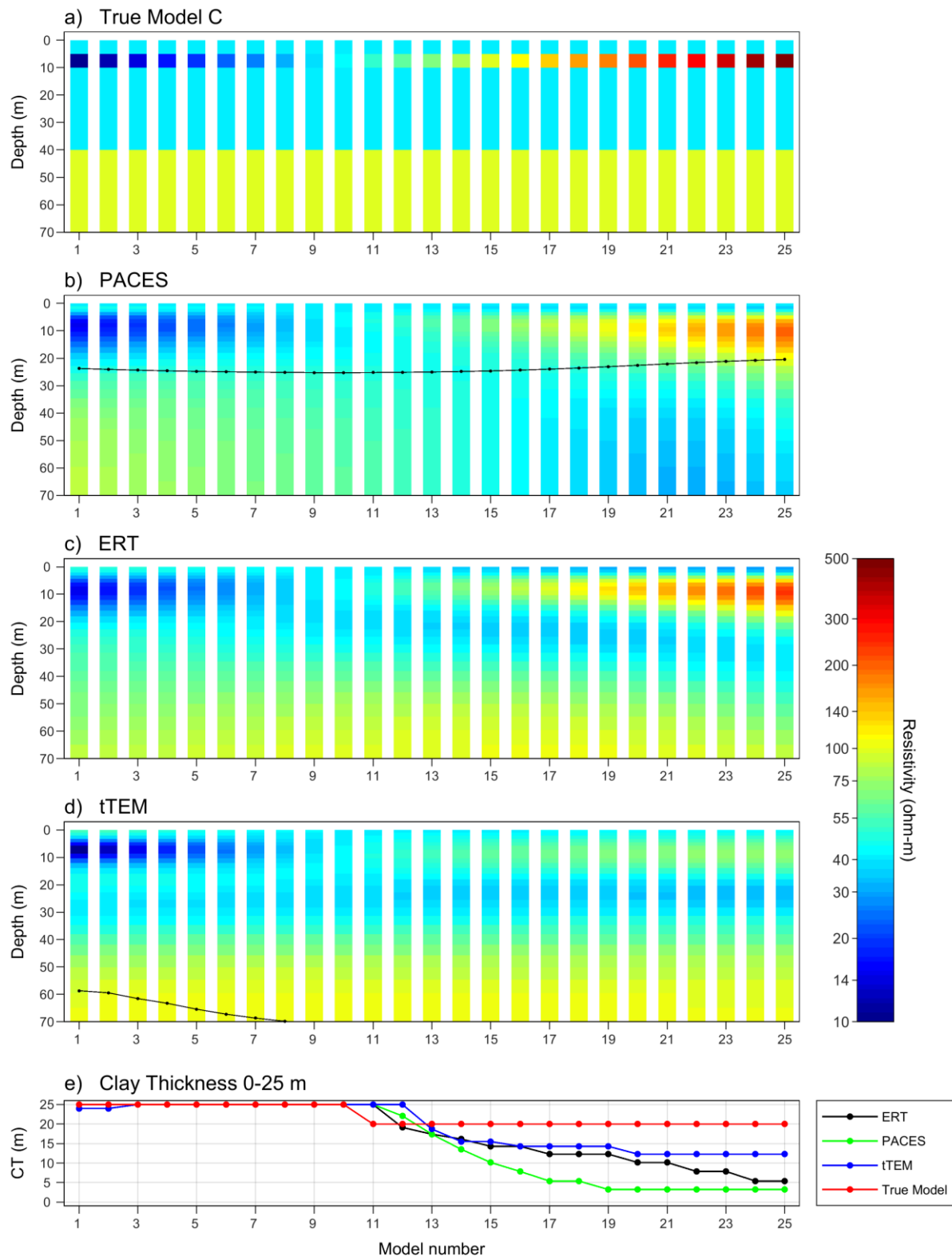


Figure 21. a) True model (40, 10-500, 40, 100  $\Omega m$ , 5, 5, 30 m). b) PACES, c) ERT, d) tTEM inversions. Black lines indicate DOI. DOI for ERT plots deeper than 70 m. e) Clay thickness 0-25 m.



The key observations of Figure 22, where layer two is placed in a resistive sandwich of  $80 \Omega\text{m}$  are similar to the previous model sweeps:

- tTEM resolves layer two better than the DC-methods in the conductive end of the model sweep.
- In the resistive end, tTEM cannot resolve the high resistivity layer sequence and provides an average resistivity of the top layer sequence.
- The DC-methods resolve layer two equally well in the conductive and resistive end of the model sweep.
- tTEM provides singly better ACT-estimates, than ERT.

Appendix 4 holds additional model sweeps with similar layout as the presented ones, and also present sharp inversions of the model sweeps presented in this section.

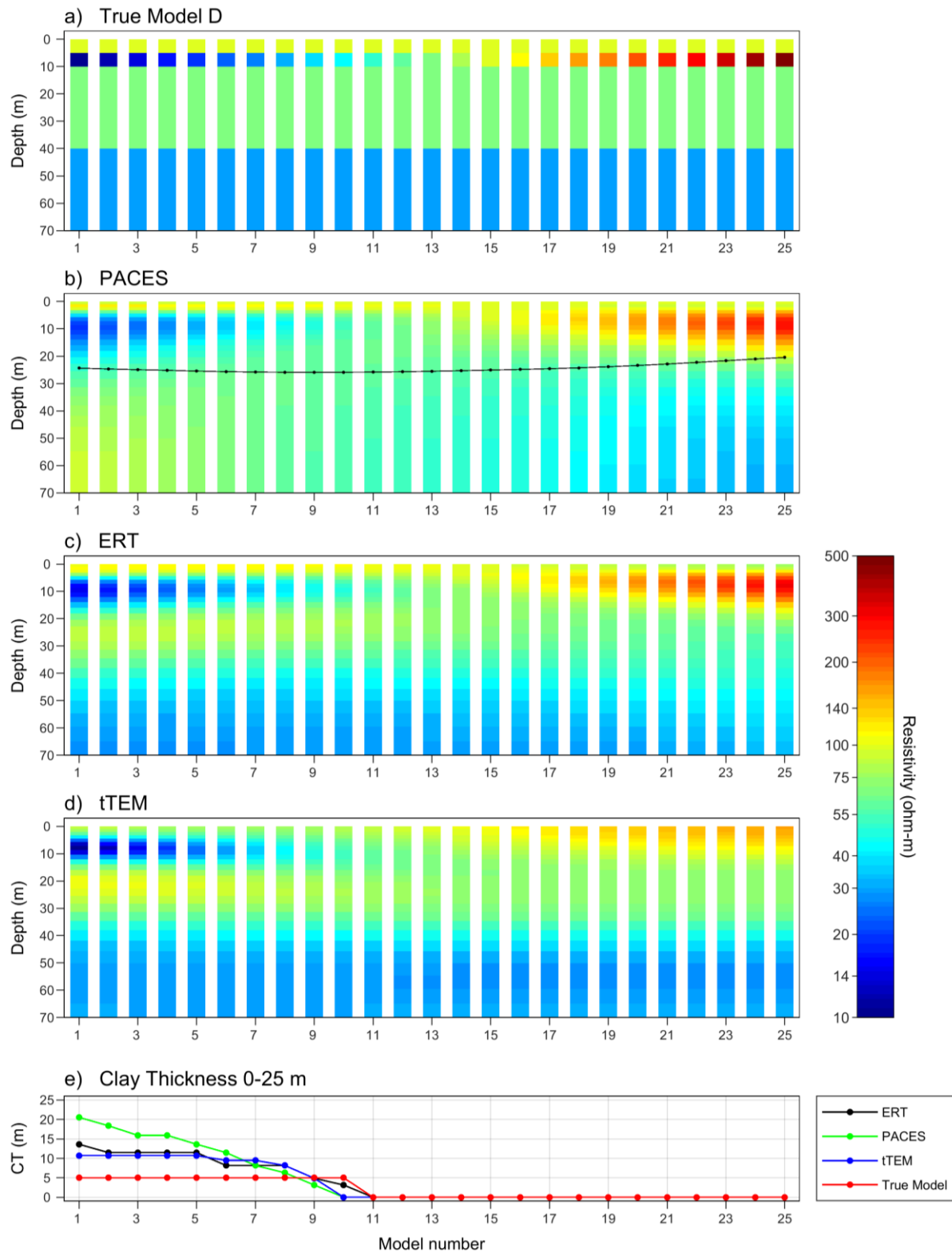


Figure 22. a) True model (80, 10-500, 80, 30  $\Omega m$ , 5, 5, 30 m). b) PACES, c) ERT, d) tTEM inversions. Black lines indicate DOI. DOI for ERT and tTEM plots deeper than 70 m. e) Clay thickness 0-25 m



## 6 MAPPING EXAMPLES – METHODS COMPARISON

To demonstrate how different or alike tTEM mapping results are compared to ERT and PACES, we have picked some areas that have been mapped with both tTEM and PACES or ERT.

Geological interpretation and further use of the PACES mapping results have most often been carried out based on interpolated mean resistivity maps in different depth intervals, and not so often directly on the 3-layer resistivity sections that appear blocky and irregular in a complex geological setting. Despite this, we will compare PACES and tTEM both on sections and area wise, hereby obtaining a better insight into the differences in the lateral resolution on the survey scale. The tTEM-ERT comparisons will only be on sections.

### 6.1 TTEM AND PACES – OURE SURVEY

The dark blue dots in Figure 23 mark the PACES lines of the Oure PACES survey. The PACES survey is from 1999, and the PACES mapping results presented here are based on the original 3-layer inversion of the dataset as downloaded from the national geophysical database – GERDA. In the different comparison examples, we will focus on the top ~25 m where PACES provides resistivity information.

The light blue dots in Figure 23 mark the tTEM lines of a newly conducted tTEM survey (2019). The tTEM setup, data processing and inversions for the survey are as described in chapter 2, and we used the smooth inversion of the tTEM dataset for the comparison. The data residuals (the data fit) for each model of the tTEM and PACES inversions inside the focus area (the dashed polygon in Figure 23) are shown in Figure 24.

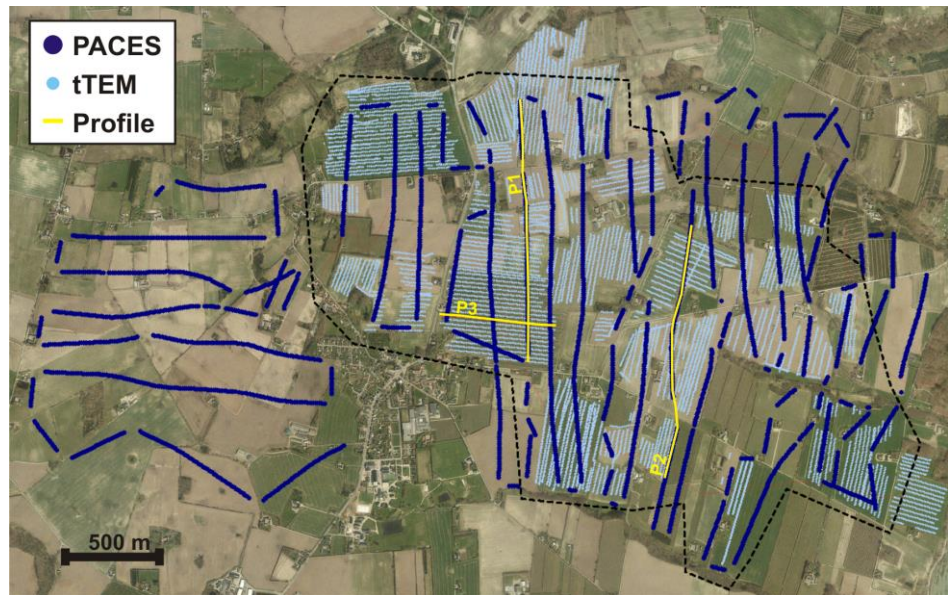


Figure 23. *t*TEM and PACES survey at Oure, South Funen. Dark blue dots mark the 1999 PACES lines. Light blue are the 2019 *t*TEM lines. A dashed polygon is used as a cropping mask for the mean resistivity maps in Figure 30 and Figure 31. Yellow lines mark the locations of three profiles. Fields inside the polygon not covered by *t*TEM could not be accessed due lack of permission.

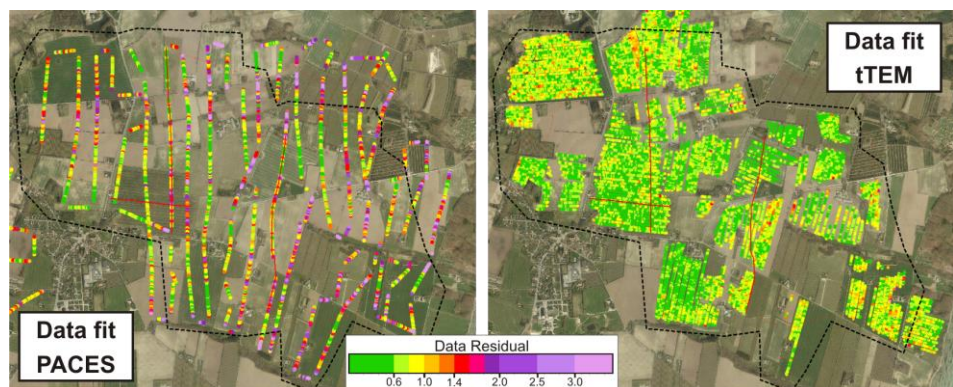


Figure 24. Data residual (data fit) for the *t*TEM and PACES inversions. The data residual is calculated as a least squares difference between observed data and forward data in log space normalized with the data uncertainties. Hence, a data residual of one corresponds to a fit similar the data uncertainty. The thin red lines mark three profiles (see Figure 23).



### Sections

Comparisons of the PACES and tTEM results are carried out along the three profiles marked in Figure 23. Profile 1 and 2 follow two PACES lines, while profile 3 follows a tTEM line.

The PACES and tTEM resistivity sections of the 1.4 km long profile 1 are shown in Figure 25. Abstracting from the dissimilarities caused by the use of different inversion model types (3-layer model vs. smooth), we see that the two methods roughly agree on the overall resistivity structures above the PACES DOI line.

At profile coordinate 900-1200 m we have a layer sequence of high-low-high resistivities, and the two methods provide similar layer thicknesses as well. The deeper conductive layer seen in the tTEM section from ~15 mbsl and deeper, is not present in the PACES section since the layer is below the PACES DOI.

As for the synthetic examples shown previously, the tTEM gives a clearer indication of low-resistivity layers in the model sequence. This is apparent for example around coordinate 200 m.

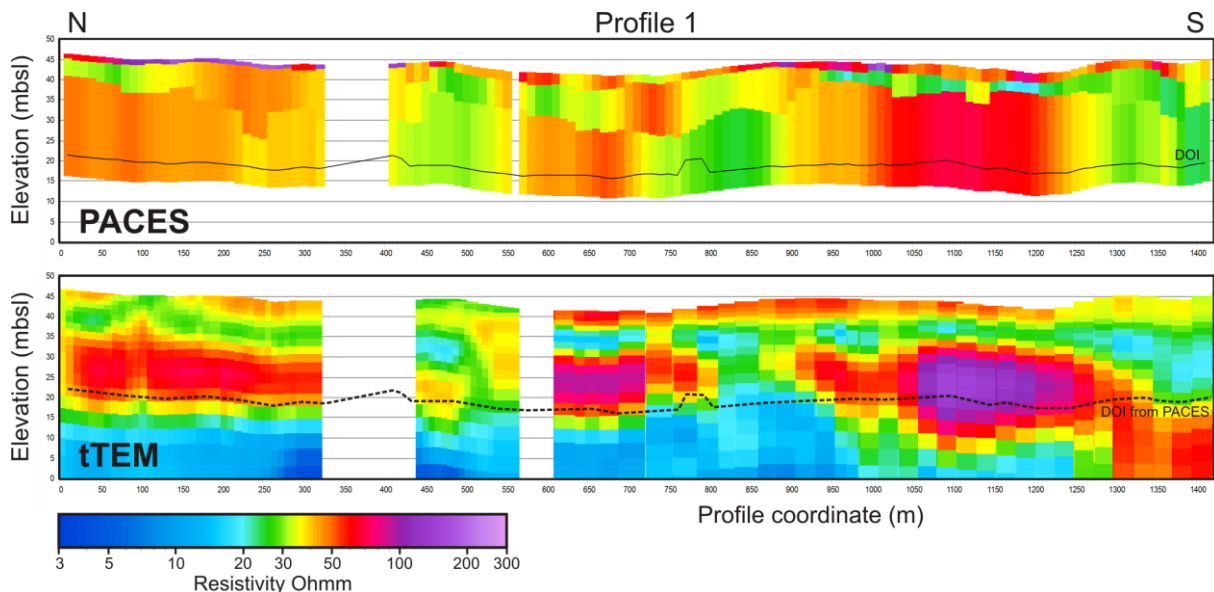


Figure 25. PACES and tTEM Resistivity sections of Profile 1. The PACES DOI line plotted is replicated as a dashed line on tTEM section. The tTEM DOI is well below the plotting window.



For PACES, the section in Figure 25 represents the maximum lateral resolution to be obtained with the PACES system, since the section follows a PACES survey line, while in the tTEM case, from profile coordinate 600-1400 m, it represents the minimum lateral resolution, since the profile runs perpendicular to the tTEM survey lines. Despite this, it seems that tTEM has an equally good or better lateral resolution than PACES. Besides that tTEM is surveying much deeper than PACES, tTEM seems to have an equally good vertical resolution as PACES in the very shallow part (0-15m).

As shown in Figure 26 b) each PACES sounding contains eight data points while a tTEM sounding consists of approximately 24 data points, and therefore offers more data to support a single tTEM model than a PACES model.

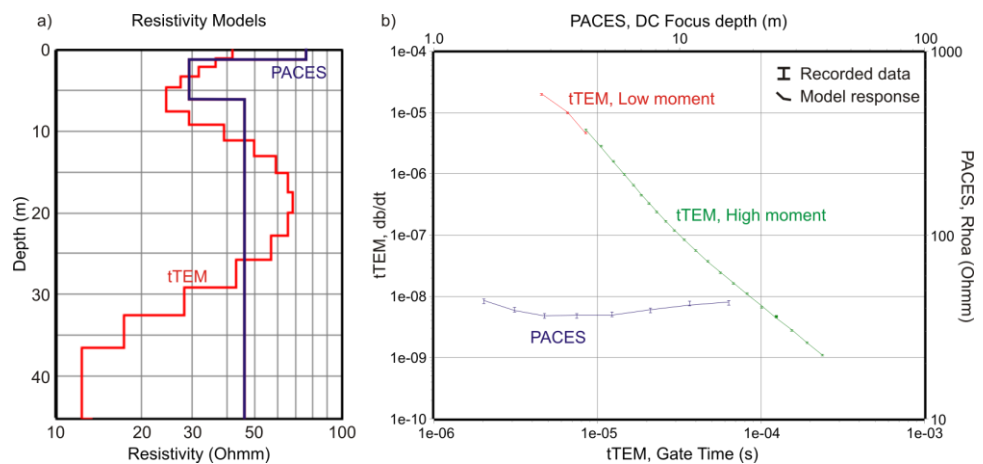


Figure 26. a) PACES and tTEM models from profile 1, Figure 26 at profile coordinate 60 m. b) Data curves and data fit for the PACES and tTEM models.

The second comparison example is shown in Figure 27. The overall structures are similar above the PACES DOI-line, but the agreement on the layer thicknesses for the top layer(s) is not as good as in the previous example. In the middle part of the section for example, the top conductive layer is thicker and less conductive in the PACES case than in the tTEM case. The opposite is observed in the right side of the section (1000-1300m) where the two top layers are thinner with PACES than in the tTEM models. Based on the tTEM result, the geology seems more complex in the left side of the section, making the three-layered PACES result difficult to interpret in this part.

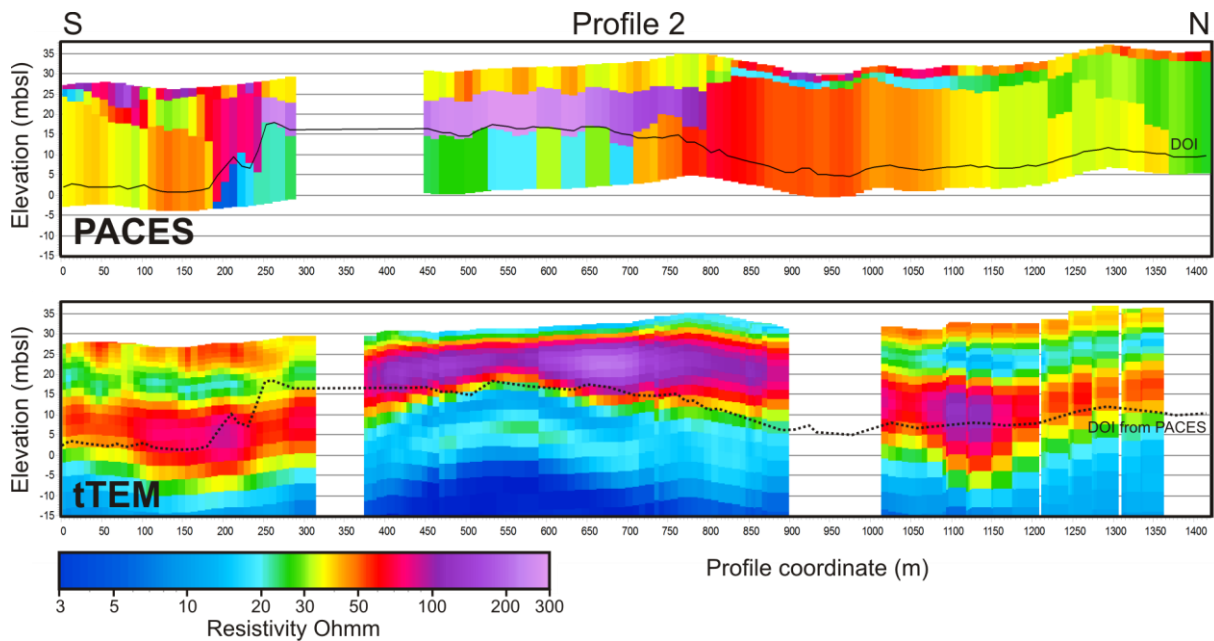


Figure 27. PACES and tTEM Resistivity sections of Profile 2. The PACES DOI line plotted is replicated as a dashed line on the tTEM section. The tTEM DOI is well below the plotting window.

Profile 3 in Figure 28 follows a tTEM line and runs perpendicularly to the PACES lines. This example is primarily included to demonstrate the lack of lateral resolution in the PACES case, due to the PACES line spacing of typically 200-300 m. As the section shows, tTEM is superior in regarding the lateral resolution, and the structures observed in the tTEM section can obviously not be reconstructed based on the few PACES models when the line spacing is 200-300 m.

We will examine the lateral resolution closer when we look at depth slices in the next section.

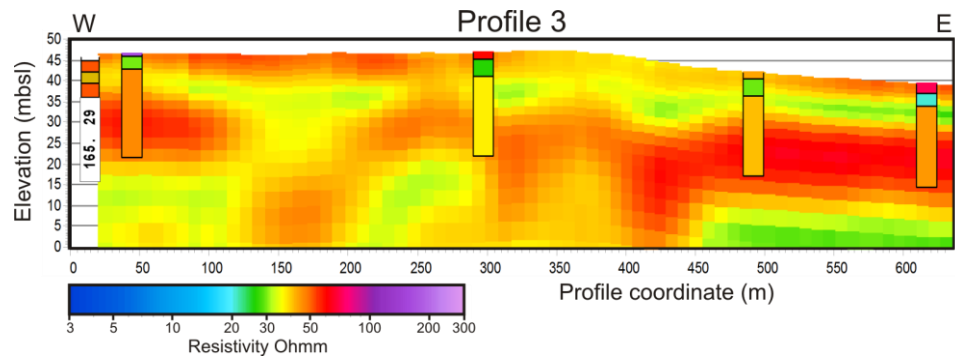


Figure 28. Resistivity sections of Profile 3. *t*TEM is the background resistivity section, front bars are PACES models. For the borehole at the west end (DGU 165.29) represents red color sand and orange color clay till.

### Areal mapping

As mentioned, the results from a PACES survey have most often been used in the form of mean resistivity maps at different depth intervals and for compiling accumulating clay thickness maps as described in section 3.4. Figure 29 therefore shows the mean resistivity in the depth interval 5-10 m for PACES plotted on top of the *t*TEM mean resistivity values. The mean resistivity values for the two methods in this interval are relatively consistent on the larger elements, e.g. for the two PACES lines at the **A**-marking in Figure 29. It is clear from Figure 29 that *t*TEM has a much higher lateral resolution than PACES, primarily due to the approximately 10 times denser line separation. For example, the finer structures in the *t*TEM result at the **B**-marking cannot be resolved by PACES as a consequence of PACES's line spacing. It is clear for the area to the left of the polygon, where only PACES is present (mark **C**) that the lateral resolution perpendicular to the PACES line is limited to the line spacing.

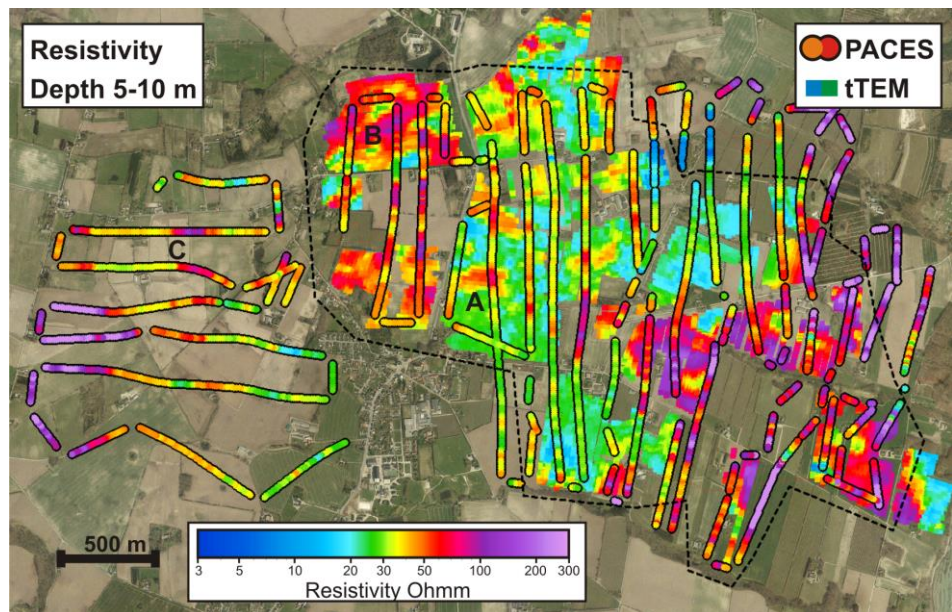


Figure 29. PACES and tTEM mean resistivity map in the depth interval 5-10 m. Black outlined dots are the PACES mean resistivity, while the background resistivity squares are the tTEM mean resistivity. The mean resistivity is calculated as a 'horizontal' mean resistivity =  $1/(\text{mean conductivity})$

Interpolated mean resistivity maps in 5 m depth intervals from 0-25 m for PACES and tTEM are presented in Figure 30 and Figure 31. The mean resistivity maps are cropped to the polygon of Figure 23 to have fair data coverage for both methods. From the mean resistivity maps, we can observe the following:

- Down to 20 m the overall resistivity structures and resistivity ranges are alike for the two methods.
- For the last interval (20-25 m) the mismatch is higher, but we are also close to or below the DOI of PACES.
- The tTEM maps contain much finer details than the PACES maps.
- A minor trend is observed in conductive areas ( $>30 \Omega\text{m}$ ) being more massive and more conductive for tTEM than for PACES, e.g. observed in the depth interval 5-10 m.
- The PACES and tTEM results seem more alike for the mean resistivity maps than with the section view. This greater likeness is a result of the mean resistivity calculation, which to some degree transforms the three-layered PACES models into smooth models more similar to tTEM models.

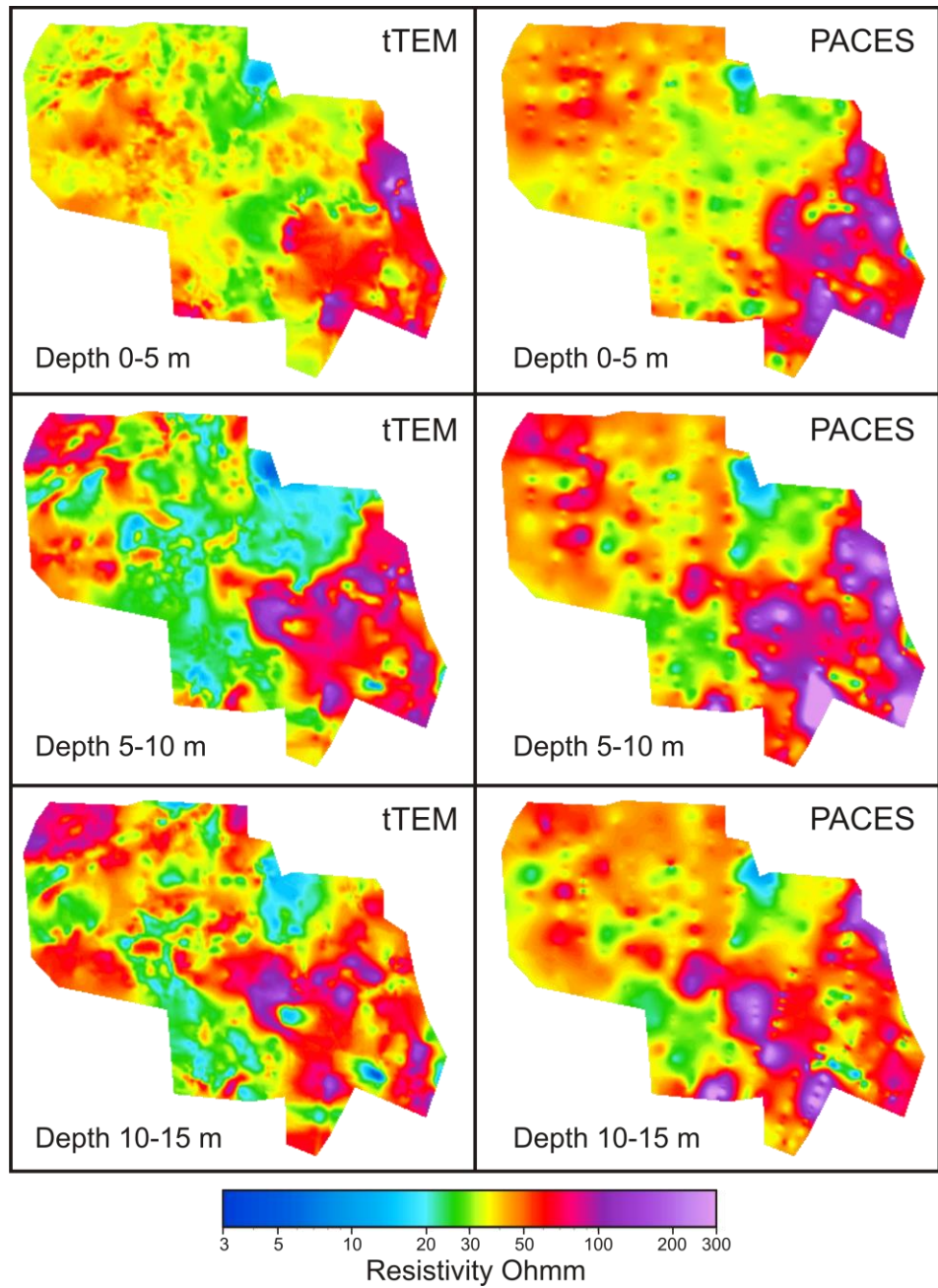


Figure 30. *t*TEM and PACES mean resistivity maps in 5 m depth intervals (0-5-10-15m). The PACES model was blanked at the DOI prior to the kriging interpolation. The mean resistivity is calculated as a 'horizontal' mean resistivity =  $1/(\text{mean conductivity})$ . The map area is approximately 3 x 2.5 km.

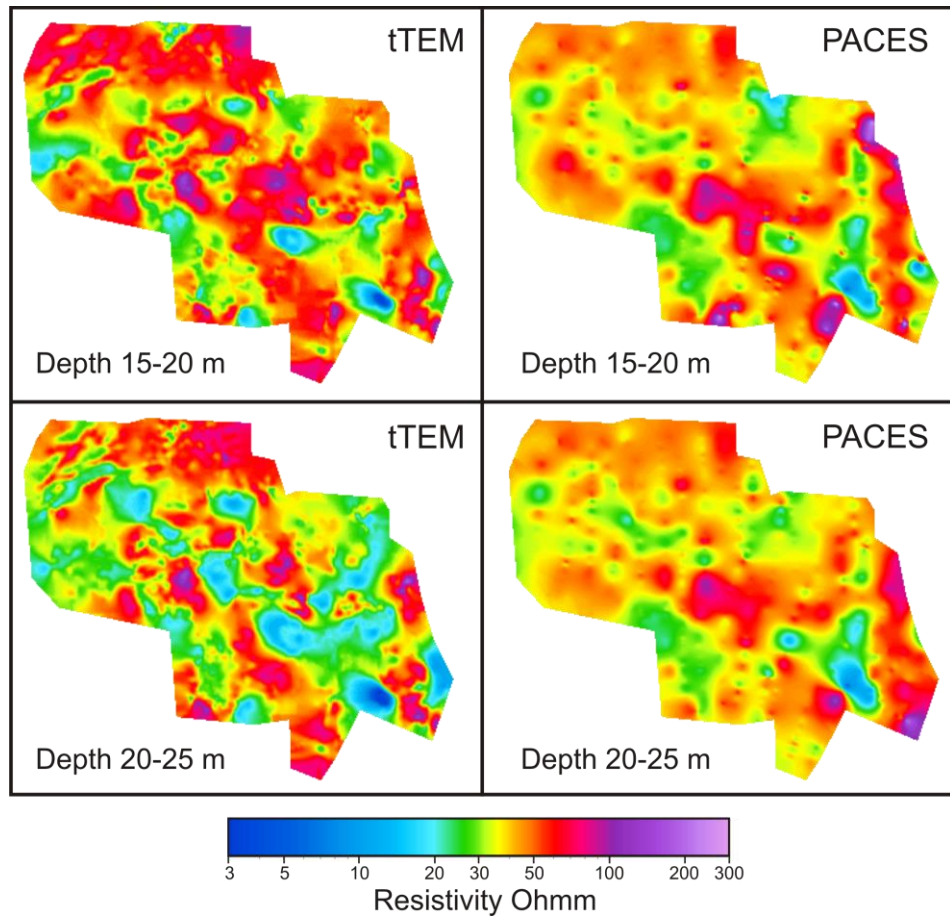


Figure 31. *t*TEM and PACES mean resistivity maps in 5 m depth intervals (15-20-25m). The PACES model was blanked at the DOI prior to the kriging interpolation, this impacting primarily the intervals 20-25m. The mean resistivity is calculated as a 'horizontal' mean resistivity =  $1/(\text{mean conductivity})$ . The map area is approximately 3 x 2.5 km.

The last PACES- *t*TEM comparison example is done with respect to the ACT. ACT maps have traditionally been compiled to a depth of 30 m, but since the PACES DOI is ~25 m and does not exceed 30 m for any of the models in this survey, the ACT is compiled for the interval 0-25 m, with a fixed translator model with upper and lower threshold values of 70 and 50  $\Omega\text{m}$  respectively.

The ACT map for *t*TEM overlain by the PACES ACT is shown in Figure 32. Based on the ACT this area is generally dominated by clay in the upper 25 m - purple color in Figure 32. The observation for this ACT comparison is similar to the mean resistivity maps. The overall match is fine, but *t*TEM has a



much finer lateral resolution than PACES, primarily due to the larger data density. A minor trend is observed towards tTEM estimates showing fewer meters of clay, than PACES in areas with intermediate ACT values, as seen at mark A and B in Figure 32. This is probably caused by conductive clay layers being better resolved and more confined in the tTEM case.

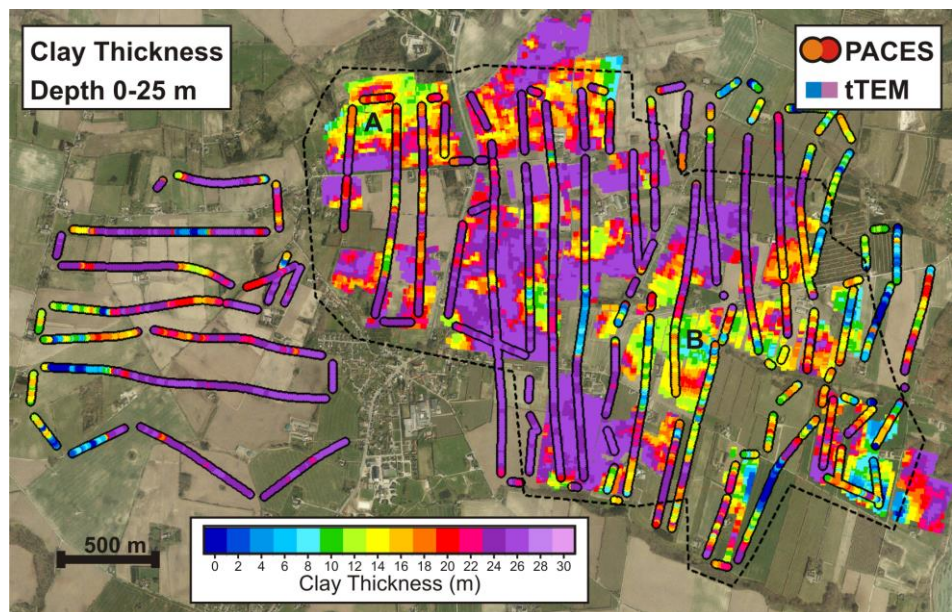


Figure 32. PACES and tTEM ACT map in depth interval 0-25 m. Black outlined dots are the PACES mean resistivity, while the background resistivity squares are the tTEM ACT map. A fixed translator model was used having upper and lower threshold values of 70 and 50  $\Omega\text{m}$  respectively (see Figure 10).

## 6.2 TTEM AND ERT – VILDBJERG, STENDAL MARK, JAVNGYDE

The ERT comparison examples in this section are from three areas in Jutland, Denmark; *Vildbjerg* located in the Central part of Jutland vest of Herning, *Stendal Mark* located in Vendsyssel south-east of Hjørring, and *Javngyde* located west of Aarhus.

Data for the five presented ERT profiles were all collected with an electrode spacing of 5 m, a 400 m electrode layout, using the roll-along technique, and with gradient array configurations. Data were processed, and inverted in 2D



in Aarhus Workbench. The data fit for the five ERT sections is normal to good. For some of the sections, IP-data were recorded as well and included in the inversion. The tTEM results are the standard smooth inversion of the datasets.

### Vildbjerg

A part of the Vildbjerg tTEM survey and the locations of two ERT profiles are shown in Figure 33, with the tTEM and ERT resistivity sections of profile 1 and 2 are shown in Figure 34 and Figure 35 respectively.

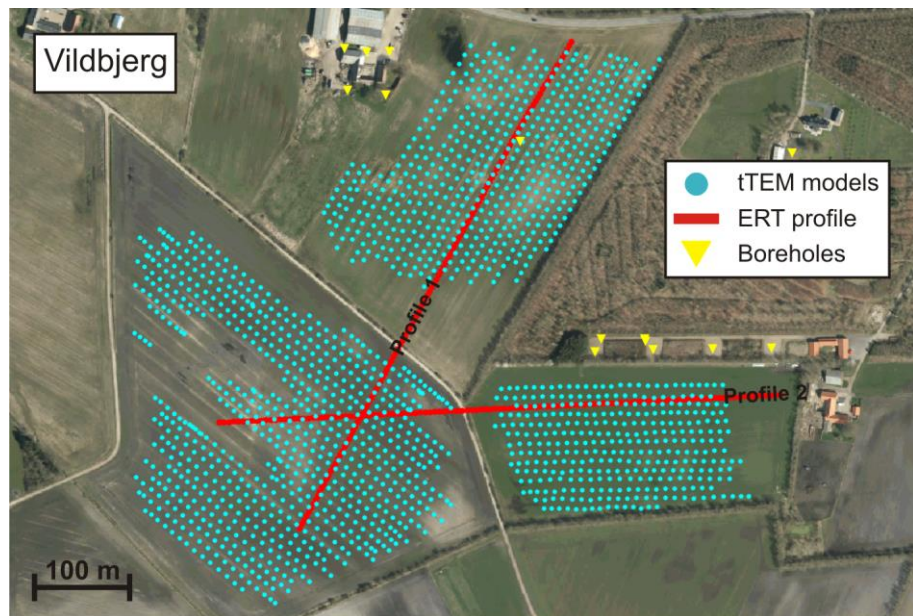


Figure 33. tTEM survey in Vildbjerg (blue dots) and location of two ERT profiles.

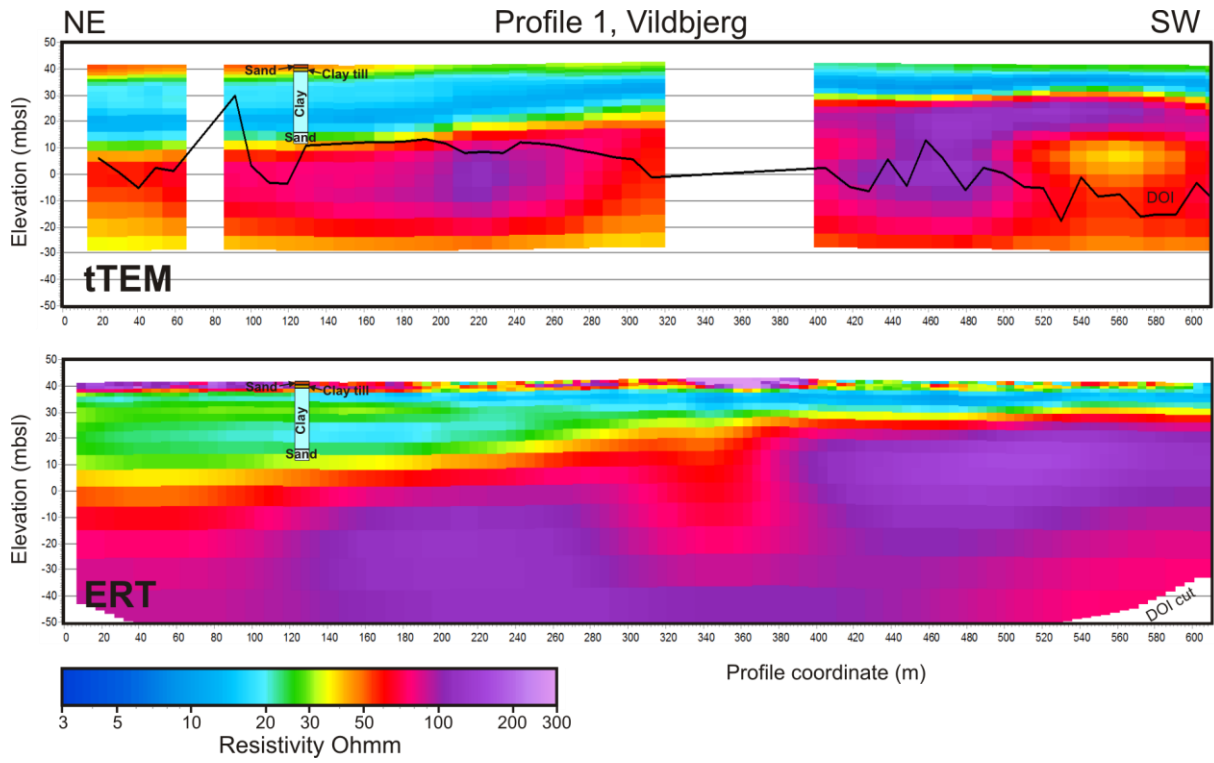


Figure 34. *t*TEM and ERT resistivity sections from Vildbjerg, profile 1, including a single borehole.

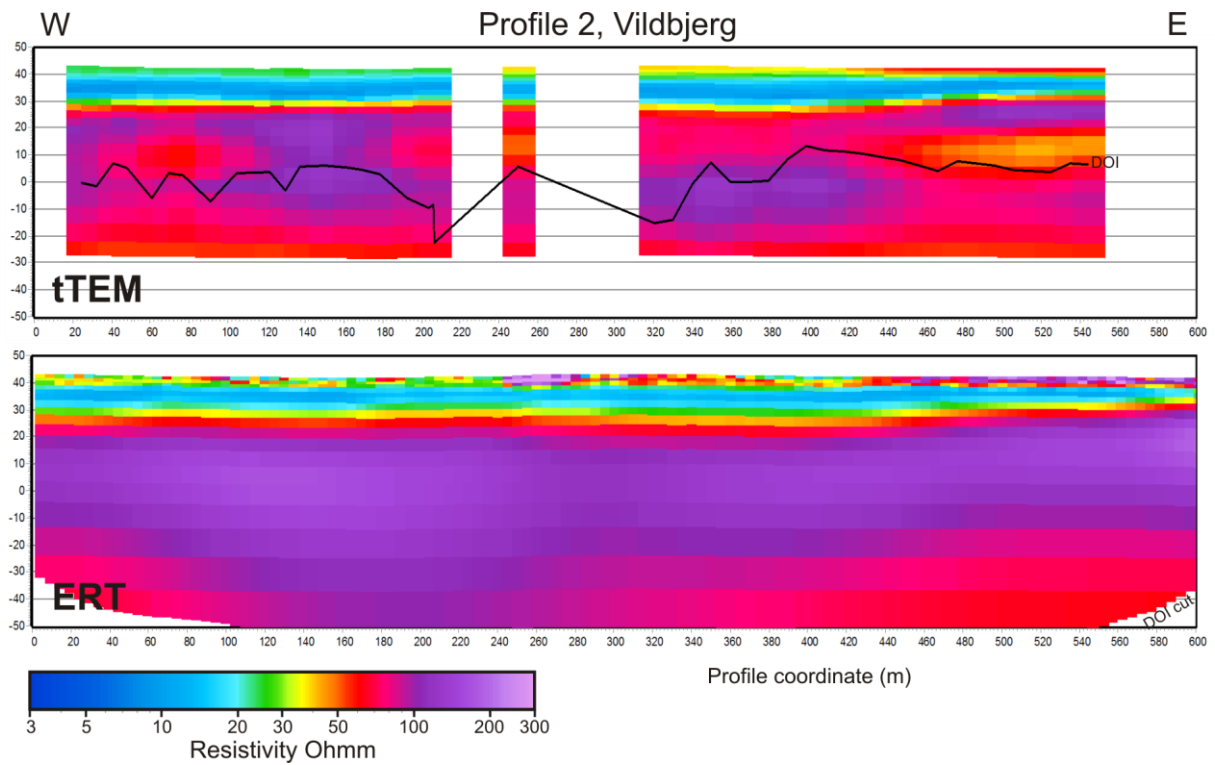


Figure 35. *t*TEM and ERT resistivity sections from Vildbjerg, profile 2.

The geology in this area is relatively layered and simple, which is also seen in the two sections. For the two profiles, we observe:

- Good correlation between the results.
- Both results match well with the borehole (profile 1) and both pick up the relatively thin shallow sand layer.
- When the top resistive sand layer becomes diffuse and/or very thin in the ERT sections it is less detectible for the *t*TEM, matching our observation regarding very thin resistive layers in the modelling study in section 5.2.
- A thick conductive layer affects the *t*TEM DOI negatively.



### Stendal Mark

The geological setting of Stendal Mark is more complex than for the Vildbjerg case. The locations of two ERT profiles in this area are shown in Figure 36. Note that profile 1 strikes almost perpendicularly to the tTEM lines and the relatively large areas with discarded tTEM data due to coupling interference (gray lines). The resistivity sections of the two profiles are shown in Figure 37 and Figure 38.



Figure 36. Part of Stendal Mark tTEM survey. Gray dots are the tTEM survey lines, overlain with the blue dots marking coupling free data invited to resistivity models. Red lines mark the two ERT profiles.

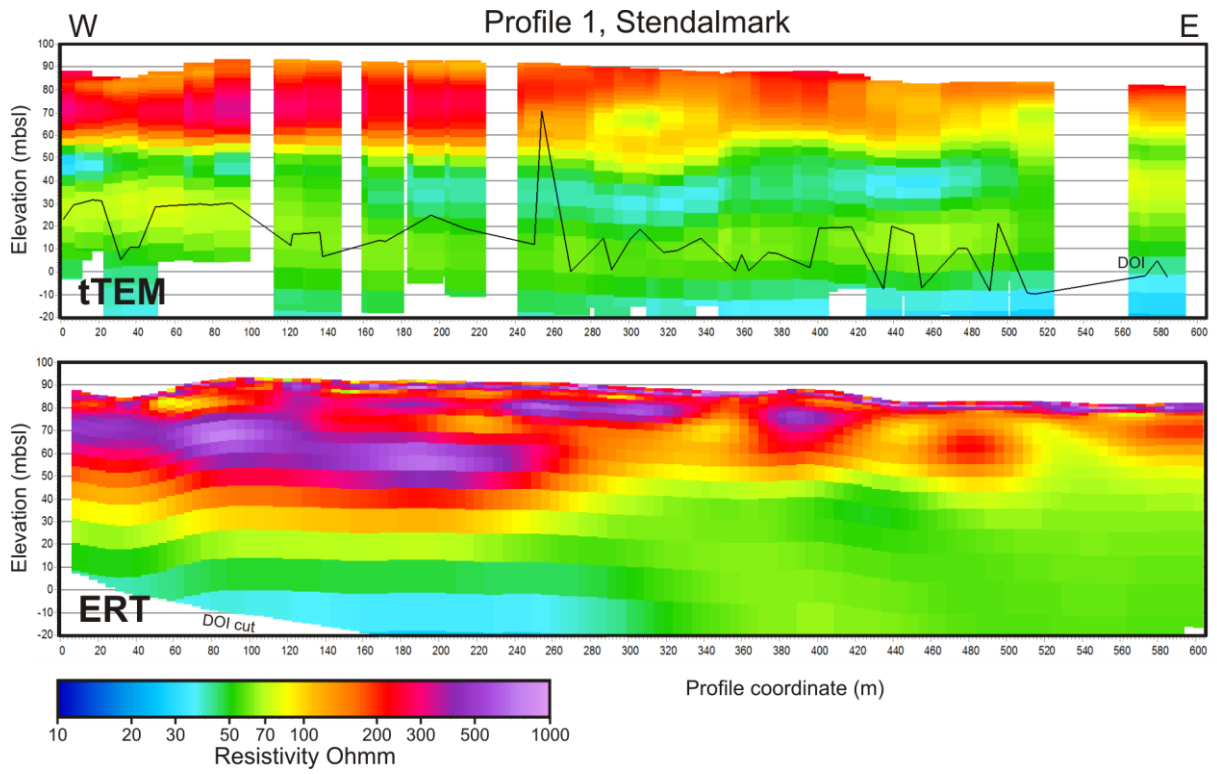


Figure 37. *t*TEM and ERT resistivity sections from Stendal Mark, profile 1.

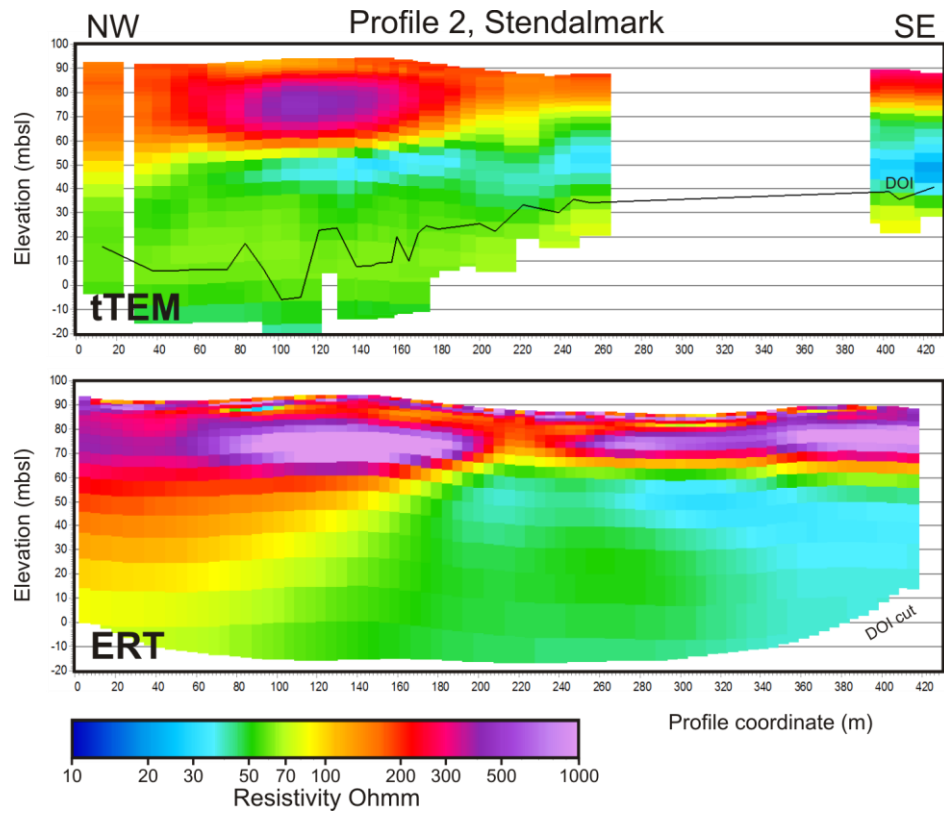


Figure 38. *tTEM and ERT resistivity sections from Stendal Mark, profile 2.*

The main observations for the Stendal Mark sections are:

- The ERT sections have more detailed and finer structures in the resistive top 25m than tTEM.
- The conductive layer at roughly 30  $\Omega\text{m}$  (light blue color) observed in the tTEM sections at elevation 50-40 mbsl is either placed deeper or not observed in the ERT sections.
- tTEM reveals more structures below elevation 50 mbsl in the resistivity range 20-60  $\Omega\text{m}$ .



### Javngyde

The geological complexity of the glacial deposit of the Javngyde area is even higher than what was seen in Stendal Mark above. The presented ERT profile was placed perpendicularly to some of the main structures observed in the tTEM results. The location of the ERT profile is shown in Figure 39, together with the tTEM lines. The tTEM section of the profile in Figure 40 is generated as a cut in a 3D resistivity grid, which results in a relatively smooth model appearance. The associated ERT section is therefore presented as an interpolated 2D grid section to achieve a similar appearance.



Figure 39. Part of tTEM survey in Javngyde (blue dots) and location the ERT profile.

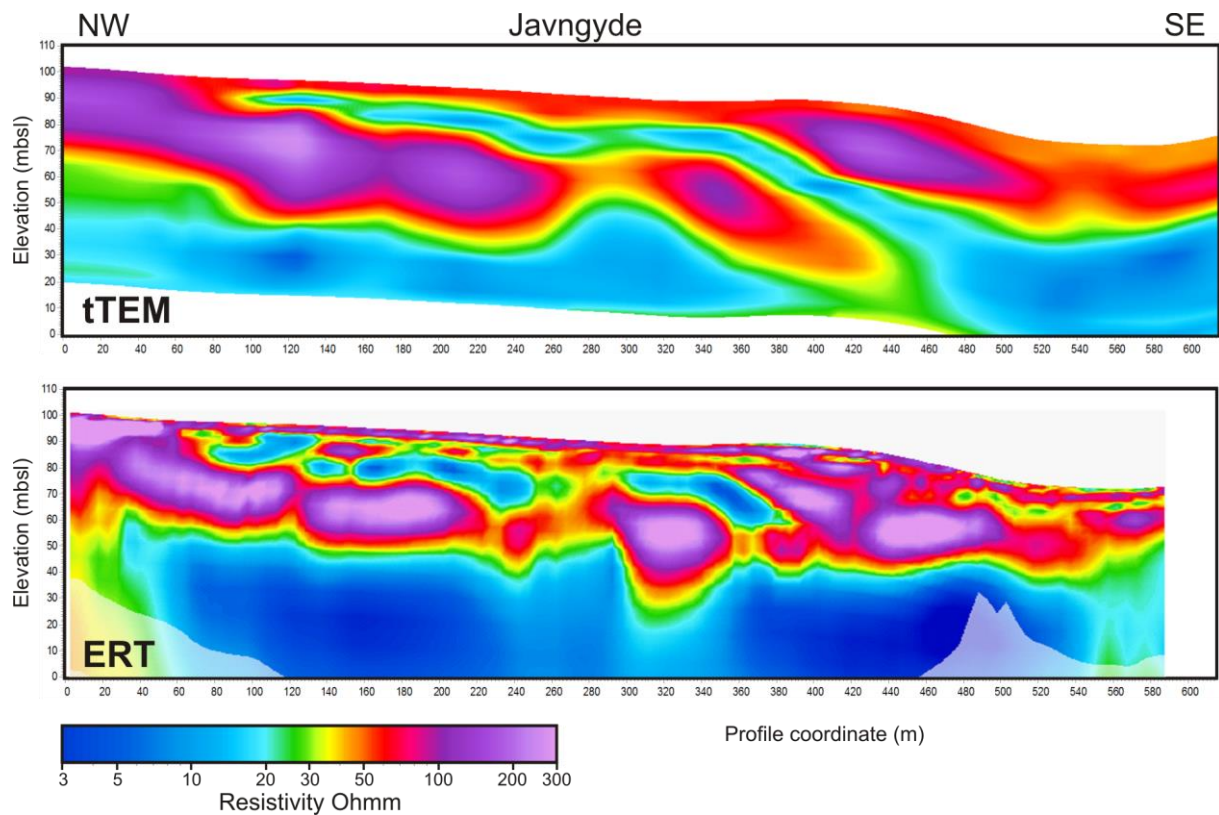


Figure 40. *t*TEM and ERT resistivity sections from Javngyde. The *t*TEM section is generated as cut in 3D resistivity grid.

From the *t*TEM and ERT section in Figure 40 we observe:

- More complex structures observed in the upper 25 m in the ERT case than in the *t*TEM case.
- The conductive bodies are more connected in the *t*TEM case resulting in quite different results at profile coordinate 350-500 m.
- Some edge effects seems to appear to the left in the deeper part of the ERT section where the conductive layer is 'missing'. This is likely due to limited data support.



## 7 DISCUSSION AND CONCLUSION

### Test site Validation

The validation at the TEM test site turned out very well. First of all, we can calibrate the tTEM system to the point reference model, which is a requirement for TEM-instruments performing geophysical mapping in Denmark. The repeatability test showed that the data repetition is excellent for the tTEM system, hence very similar resistivity sections for the repetitions. Any dissimilarities can therefore be attributed to differences in data uncertainties/noise level and/or model equivalences.

The match to the reference line response is very good in general. We observed a minor mismatch for some gate times for a minor part of the reference line, but no systematic offsets or errors for the full reference line was observed. The minor mismatches in data space to the reference data only had a minor impact in the inverted resistivity sections, also considering the different layout and footprint of the tTEM system compared to the TEM-system used for the reference section. Equally important, the test-site validation is also a validation of the processing and modelling schemes used for the tTEM systems.

The test site is routinely visited as a quality control of the tTEM systems when system changes or instrument repairs have been implemented. The site is also visited prior to larger surveys where the system is re-calibrated at the test site. Long time system drift with respect to the test-site calibration parameters is not observed. To check for small instrument related bias signals, tests on a resistive site are carried out as well.

### Model resolution

The physics behind the DC-methods, PACES, ERT and the tTEM are quite different, and hence the resolution capabilities, model equivalence issues, etc. are quite different as well. How well a given method can resolve the subsurface is therefore also very model dependent, and very specific rules like "*a layer can be resolved with tTEM if it is thicker than 3 m*", cannot be established. Based on our model resolution study and the mapping examples we can extrude some trends and make generalizations regarding the resolution for the different systems with focus on tTEM. In the statements below ERT refers to the simulated 400 m, 5 m electrode spaced ERT layout.

- Compared to PACES and ERT, tTEM is good at resolving layer sequences involving conductive layers, and less good at resolving layer sequences only involving very resistive layers.



- tTEM can resolve a conductive top layer if it is more than about 2 m thick, while the top layer needs to be minimum 3-4 m thick in the resistive case.
- For both tTEM, ERT and PACES the resolution capability decreases with depth, meaning that resistivity structures need to be increasingly larger as to depth in order to be mapped.
- ERT has a slightly better resolution than tTEM in the top 10-15 m, especially for resistive structures.
- The lateral resolution in a tTEM survey is superior to the PACES system, primarily due a much denser line spacing, but also because of a smaller footprint and more data per resistivity model.
- The DOI of tTEM is about 3-4 times larger than PACES
- The DOI of ERT is slightly larger than tTEM, but with the newer RC20 tTEM receiver coil (not used in the examples shown) we anticipate that the DOI of tTEM will become similar to that of the ERT, since the RC20 receiver coil result in a better signal-to-noise ratio.
- tTEM provides more accurate ACT estimates than PACES and ERT.

### **Perspectives**

The tTEM system has already been used intensively for mapping in Denmark, primarily in connection with the research projects rOpen, TopSoil, and MapField, where most of the tTEM system development was carried out. In these projects the tTEM mapping results have been used to generate detailed structural input to groundwater flow and transport models. Making the already completed tTEM mapping results available in the national geophysical database, GERDA, is an area of focus.

The tTEM system has also attracted a lot of interest outside Denmark. Several projects with foreign partners have already been carried out and more projects are lined up in the near future.

Due to the dense data sampling and full area coverage, the tTEM data are ideally suited for a full 3D-inversion, which will be available in the near future. For small and shallow 3D targets, 3D-inversion of tTEM data can provide accurate and high detailed mapping of the target, something that cannot be achieved to the same degree with an airborne system with a larger footprint and wider line-spacing.



## 8 REFERENCES

### tTEM-system

Status for tTEM-kortlægninger, GFS-report, April 2019

Auken, E., N. Foged, J. Larsen, K. Lassen, P. Maurya, S. Dath, and T. Eiskjær, 2018, tTEM — A towed transient electromagnetic system for detailed 3D imaging of the top 70 m of the subsurface, *GEOPHYSICS*, E13-E22.

Auken, E., J. B. Pedersen, and P. K. Maurya, 2018, A new towed geophysical transient electromagnetic system for near-surface mapping, *Preview*, June 2018, 33-35.

Behroozmand, A.A., Auken, E., Knight, R., 2019, Assessment of Managed Aquifer Recharge Sites Using a New Geophysical Imaging Method, *Vadose Zone Journal*, May 2019.

Kim, H., A. Høyer, R. Jakobsen, L. Thorling, J. Aamand, P. K. Maurya, A. V. Christiansen, B. Hansen, 2019, 3D characterization of the subsurface redox architecture in complex geological settings, *Science of the Total Environment* 693 (2019)

Maurya, P.K., A. V. Christiansen, J. Pedersen, E. Auken, 2019, High resolution 3D subsurface mapping using towed transient electromagnetic system - tTEM: case studies, submitted to *Near Surface Geophysics*.

### PACES

Sørensen, K. I., 1996, Pulled Array Continuous Electrical Profiling, *First Break*, 14, 3, 85-90.

Christensen, N. B., and K. I. Sørensen, 2001, Pulled array continuous electrical sounding with an additional inductive source: an experimental design study, *Geophysical Prospecting*, 49, 241-254.

### ERT

Dahlin, T. and Zhou, B., 2004. A numerical comparison of 2D resistivity imaging with 10 electrode arrays. *Geophysical Prospecting* 52: 379-398

Loke, M. H., Chambers, J. E., Rucker, D. F., Kuras, O., and Wilkinson, P. B., 2013, Recent developments in the direct-current geoelectrical imaging method: *Journal of Applied Geophysics*, v. 95, p. 135-156.

### TEM-test site calibration and validation

Foged, N., E. Auken, A. V. Christiansen, and K. I. Sørensen, 2013, Test site calibration and validation of airborne and ground based TEM systems, *Geophysics*, 78, 2, E95-E106.

Validation of the SkyTEM system at the extended TEM test site, 2010, GFS-report, 2010.

Refinement of the TEM reference model at Lyngby, GFS-report, June 2012.



### **ACT**

Christiansen, A. V., N. Foged, and E. Auken, 2014, A concept for calculating accumulated clay thickness from borehole lithological logs and resistivity models for nitrate vulnerability assessment, *Journal of Applied Geophysics*, 108,69-77.

Foged, N., P. A. Marker, A. V. Christiansen, P. Bauer-Gottwein, F. Jørgensen, A.-S. Høyer, and E. Auken, 2014, Large scale 3D-modelling by integration of resistivity models and borehole data through inversion, *Hydrology and Earth System Sciences*, 18,4349-4362.

### **DOI**

Christiansen, A. V., and E. Auken, 2012, A global measure for depth of investigation, *Geophysics*, 77, 4,WB171-WB177.

### **Data Processing**

Auken, E., A. V. Christiansen, J. A. Westergaard, C. Kirkegaard, N. Foged, and A. Viezzoli, 2009, An integrated processing scheme for high-resolution airborne electromagnetic surveys, the SkyTEM system, *Exploration Geophysics*, 40,184-192.

### **Inversion**

Sharp Model Inversion Setup for inversion of geophysical data - Guidelines and Examples, GFS-report, June 2018.

Lateral sambunden tolkning af transiente elektromagnetiske data, GFS-rapport, 2004 .

LCI tolkning af geoelektriske data - verificering af metoden, GFS-report 2002.

Auken, E., A. V. Christiansen, B. H. Jacobsen, N. Foged, and K. I. Sørensen, 2005, Piecewise 1D Laterally Constrained Inversion of resistivity data, *Geophysical Prospecting*, 53,497-506.

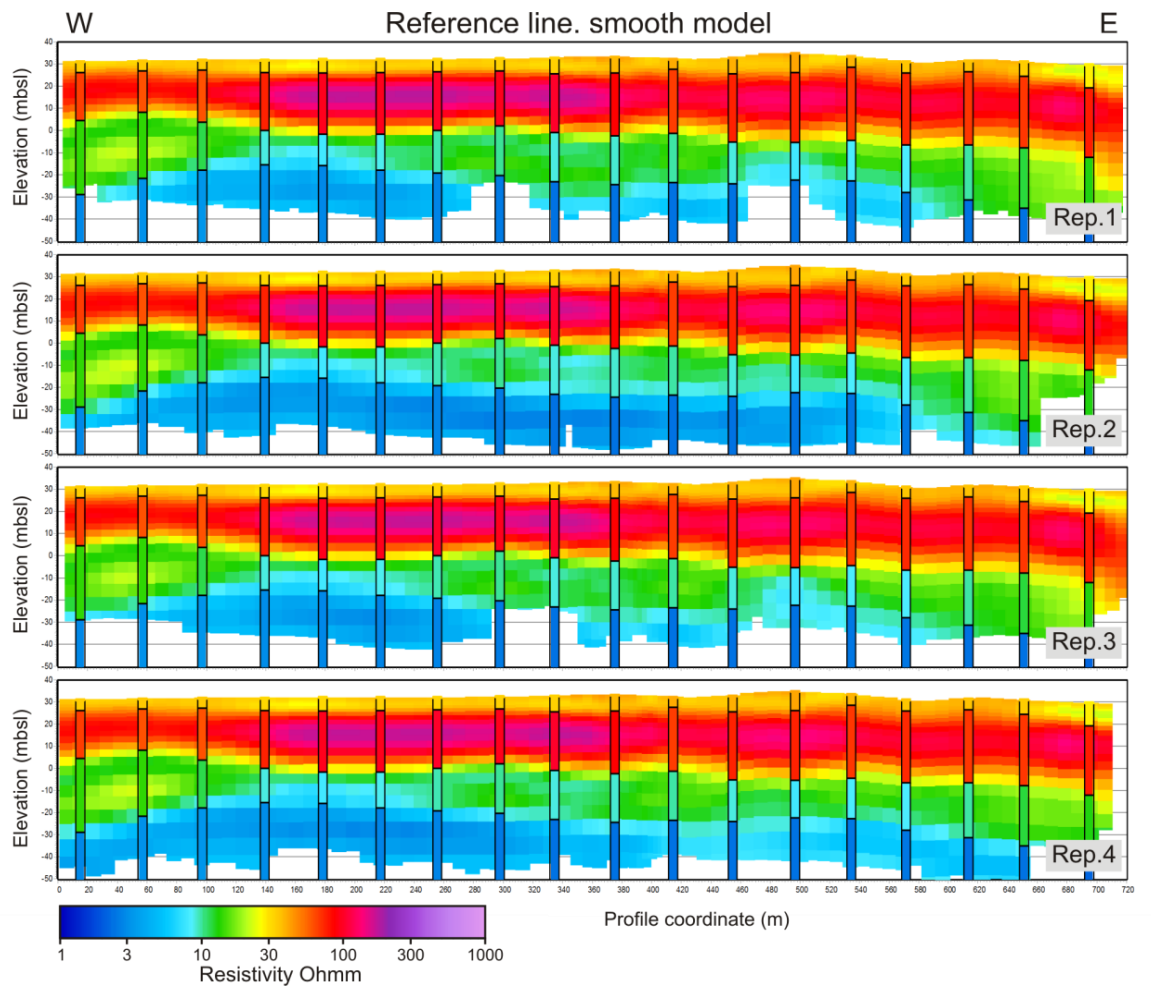
Auken, E., A. V. Christiansen, G. Fiandaca, C. Schamper, A. A. Behroozmand, A. Binley, E. Nielsen, F. Effersø, N. B. Christensen, K. I. Sørensen, N. Foged, and G. Vignoli, 2015, An overview of a highly versatile forward and stable inverse algorithm for airborne, ground-based and borehole electromagnetic and electric data, *Exploration Geophysics*, 2015, 46,223-235.

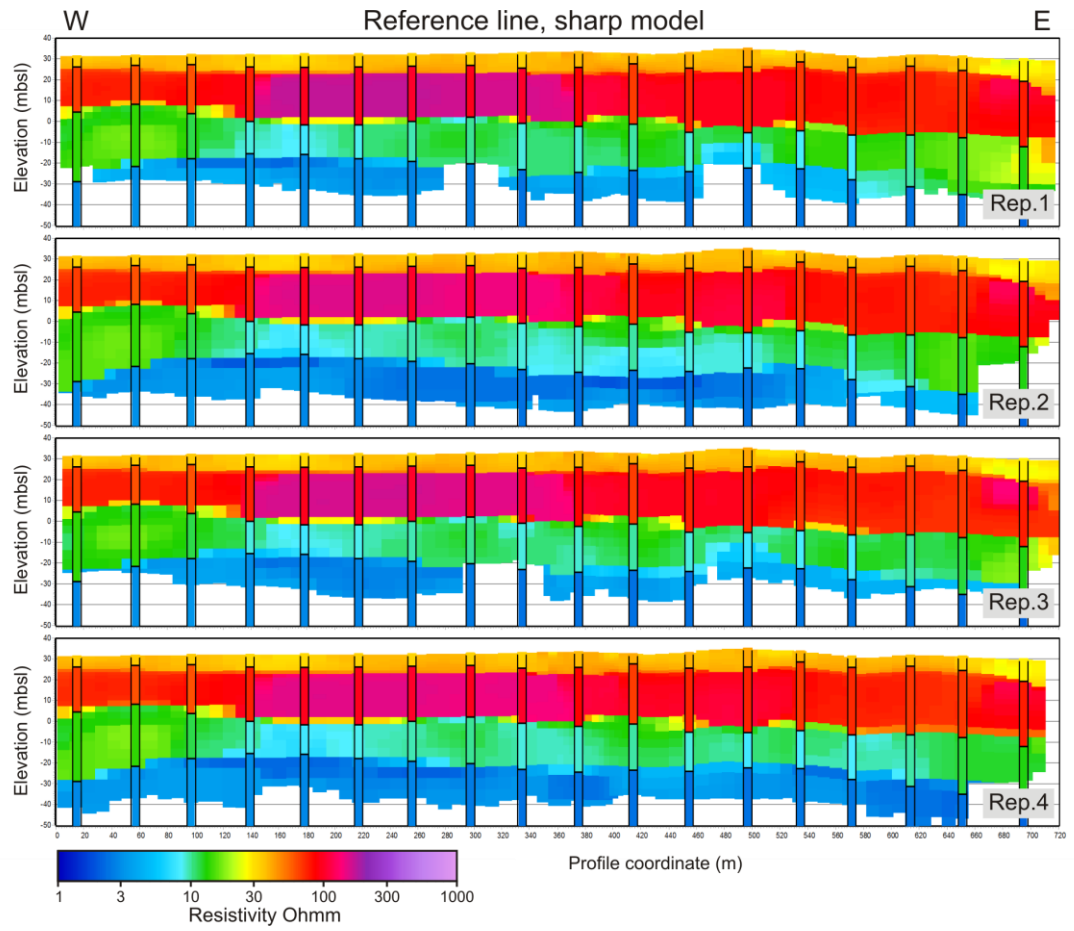
Viezzoli, A., A. V. Christiansen, E. Auken, and K. I. Sørensen, 2008, Quasi-3D modelling of airborne TEM data by Spatially Constrained Inversion, *Geophysics*, 73, 3,F105-F113.

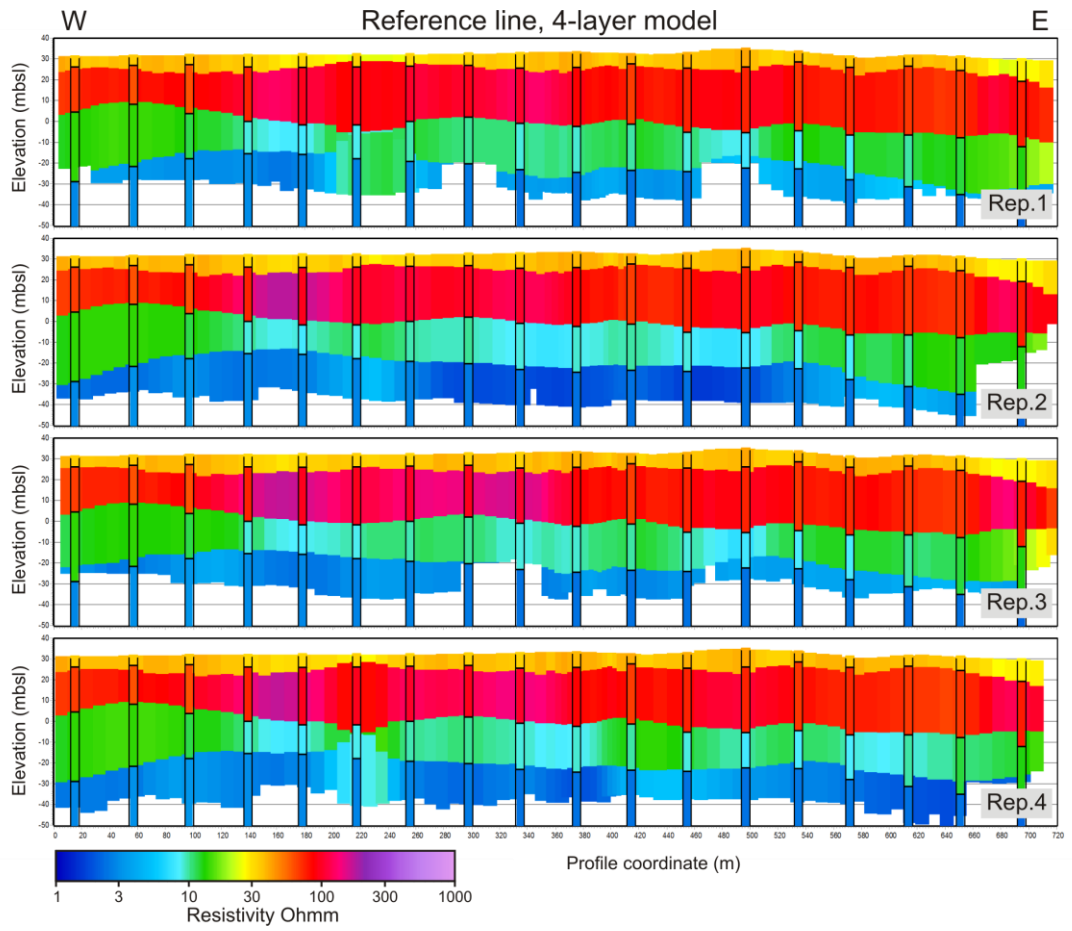


## APPENDIX 1 TEST SITE VALIDATION, MODEL SECTION

This appendix holds sharp, smooth, and four layer inversion results of the four repetitions of the reference line. The background sections are the tTEM results while the front bars are the reference models.



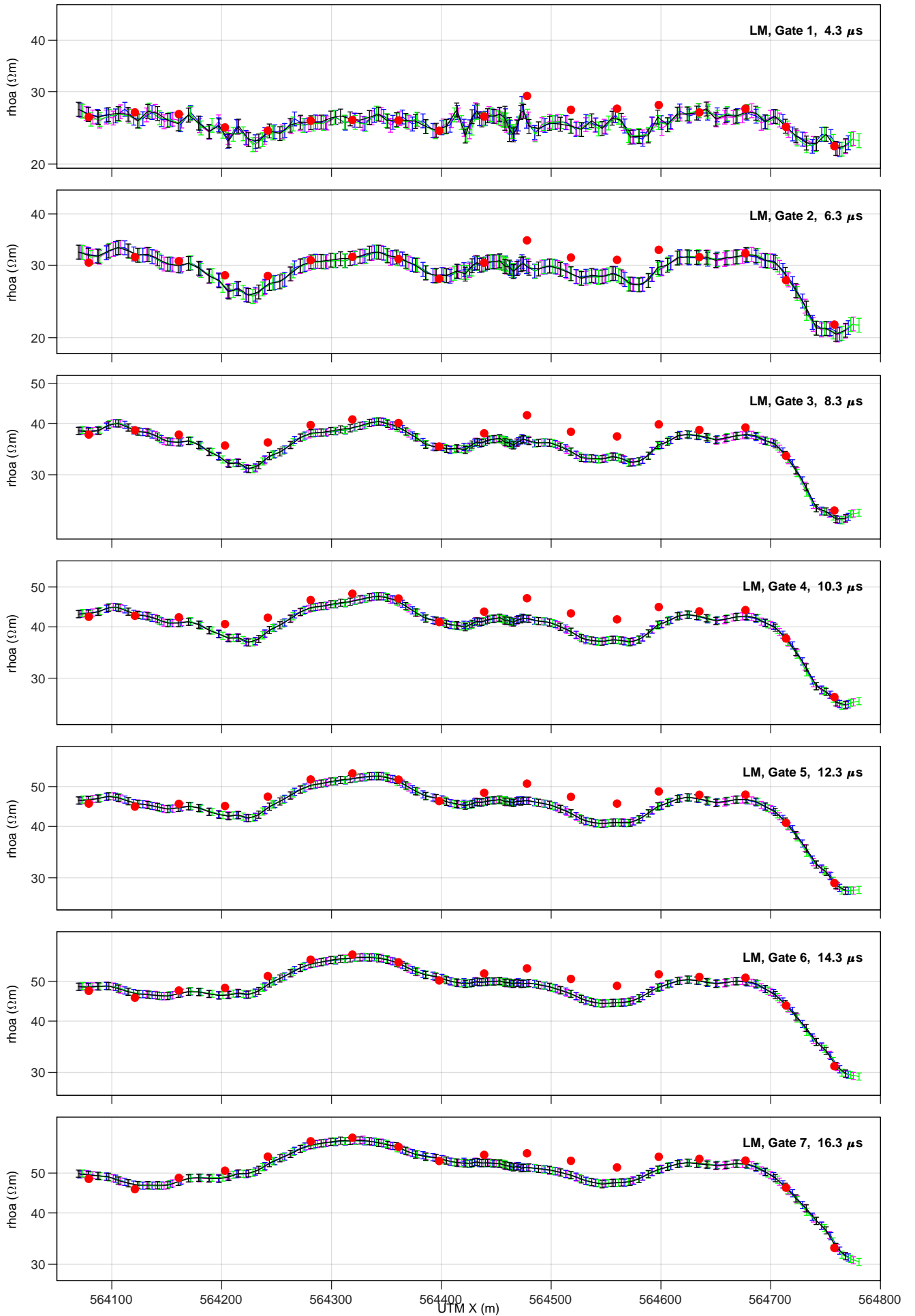


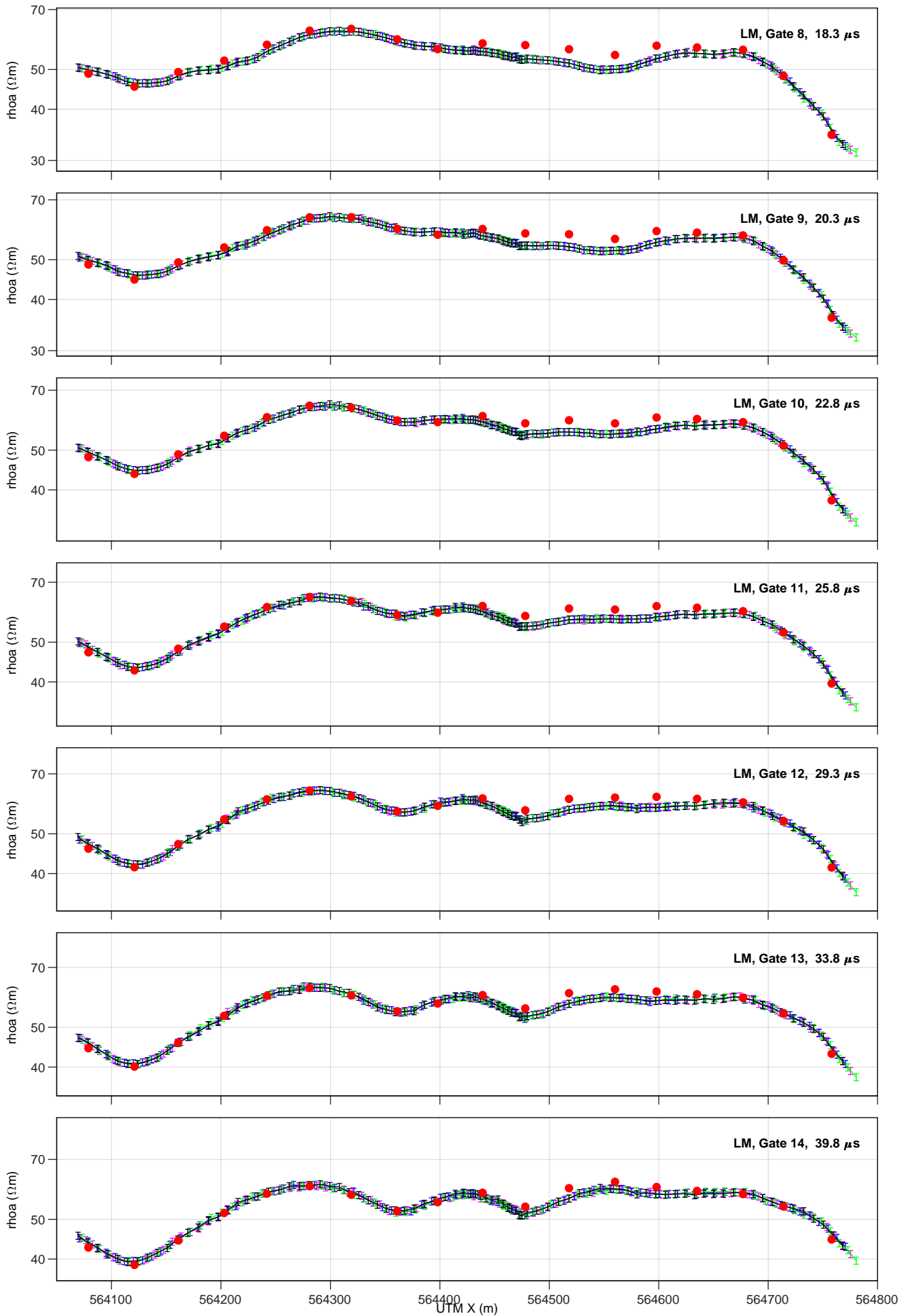


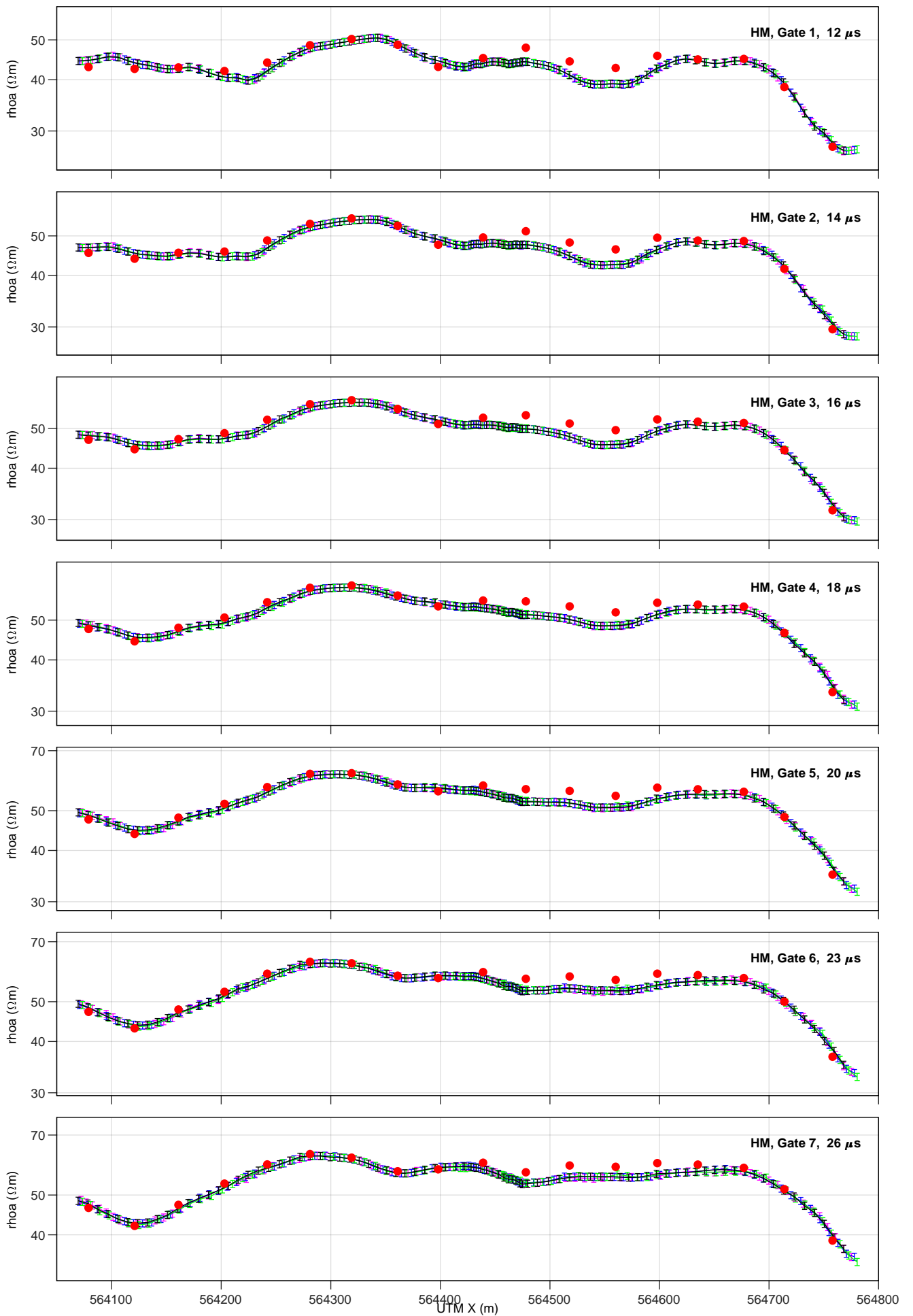


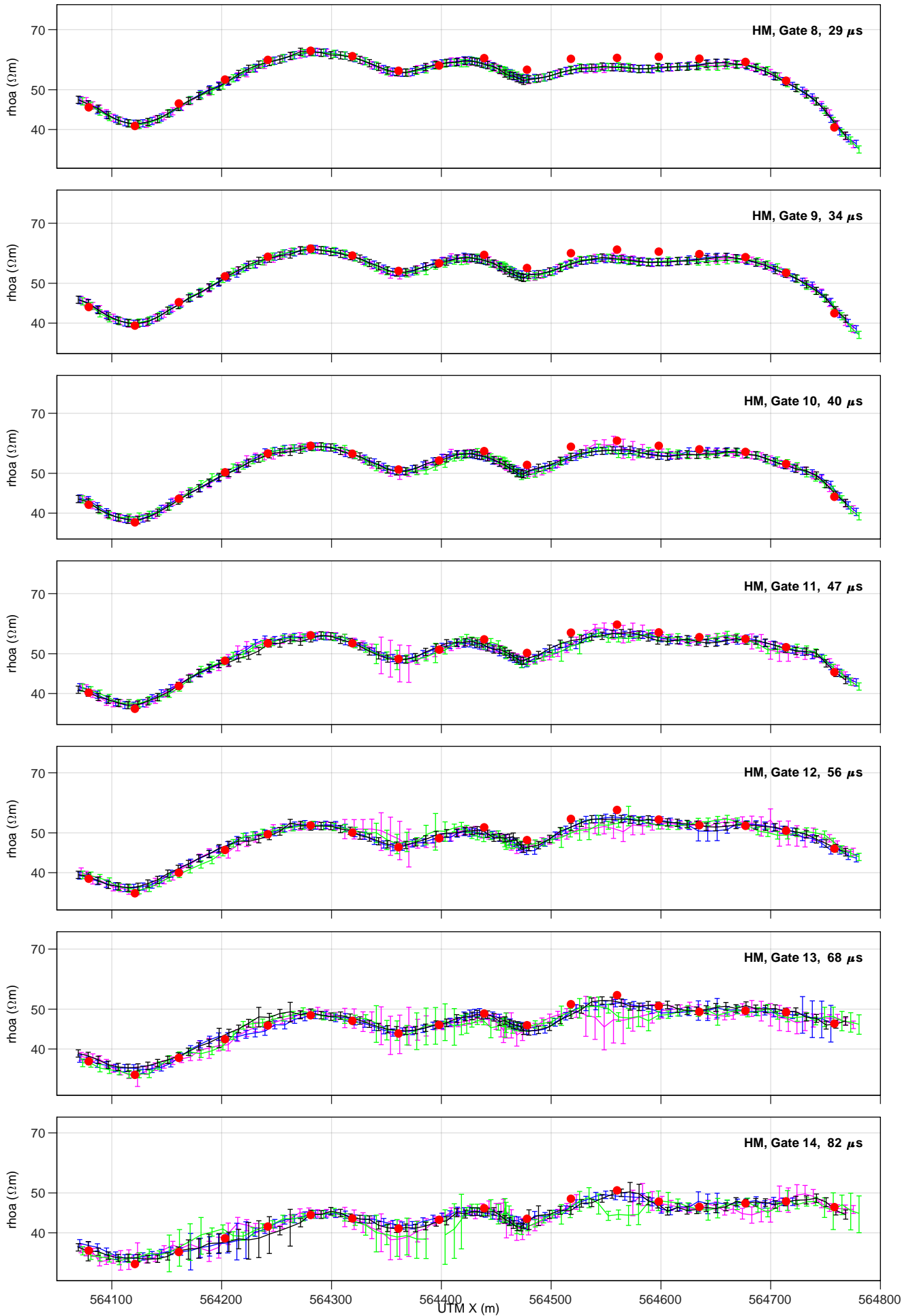
## **APPENDIX 2 TEST SITE VALIDATION, DATA PLOTS**

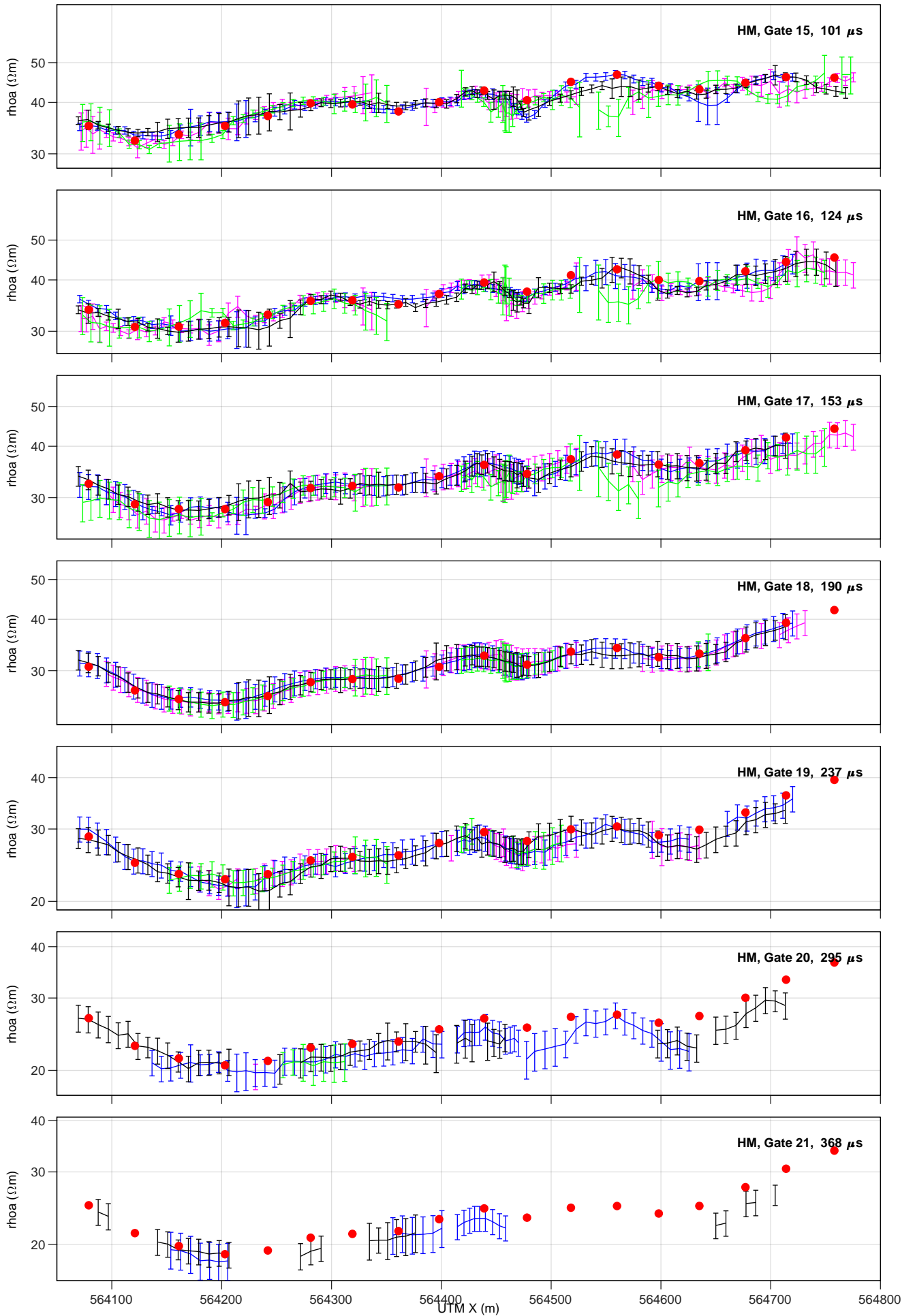
This appendix holds data plots of all LM and HM time gates from the reference line. The error bars mark the recorded tTEM data. Each color represents a line repetition. Red dots mark the reference response.













## APPENDIX 3 SETUP FILES

AarhusInv formatted system setup files for ERT, PACES and tTEM used in the modelling study.

### PACES, DCP-FILE

```
%PACES configuration
22
1 1 1 2
0.00 10.10 20.30 30.40 5.72 0.05 5.25 0.00
0.00 -19.30 49.70 30.40 6.90 0.05 10.94 0.00
0.00 -30.50 60.80 30.40 6.47 0.05 15.83 0.00
0.00 -30.50 40.60 30.40 6.32 0.05 7.61 0.00
0.00 -30.50 -2.10 30.40 5.77 0.05 1.60 0.00
0.00 -30.50 3.00 30.40 5.48 0.05 2.12 0.00
0.00 -30.50 -4.10 30.40 5.73 0.05 2.81 0.00
0.00 -30.50 25.40 30.40 5.59 0.05 3.76 0.00
```

### ERT, DCP-FILE

```
%The 24 unique config. from 5m spacing ERT profile, Gradient-array
22
1 1 1 2
0 5 10 45 123 0.05 2.68 9.31
0 10 15 45 123 0.05 5.08 13.47
0 70 80 90 123 0.05 5.36 78.62
0 15 20 45 123 0.05 7.48 17.92
0 20 25 45 123 0.05 8.54 22.50
0 60 70 90 123 0.05 10.16 66.93
0 50 60 90 123 0.05 14.96 55.85
0 30 70 340 123 0.05 16.85 33.49
0 40 50 90 123 0.05 17.08 45.00
0 40 80 360 123 0.05 21.44 45.54
0 110 120 170 123 0.05 23.56 115.93
0 100 110 170 123 0.05 28.15 105.58
0 60 80 260 123 0.05 28.82 66.82
0 90 100 170 123 0.05 31.36 95.28
0 80 90 170 123 0.05 32.49 85.00
0 230 270 340 123 0.05 36.02 258.68
0 80 100 260 123 0.05 38.78 88.11
0 240 280 360 123 0.05 40.66 267.72
0 100 120 260 123 0.05 46.65 109.11
0 120 140 260 123 0.05 49.56 130.00
0 110 150 340 123 0.05 55.56 126.23
0 120 160 360 123 0.05 59.82 136.60
0 150 190 340 123 0.05 64.20 170.00
0 160 200 360 123 0.05 68.31 180.00
```



## TTEM, LOW MOMENT, TEM-FILE

```
%tTEM, Low moment
72 3
0.00 0.00 -0.50 -9.53 0.00 -0.30
  4 8.00
-02.00 -01.00
  02.00 -01.00
  02.00 01.00
-02.00 01.00
3 3 3
3 1
39 ... 2.2438e-06 2.8000e-06 1.1000e-02 0.0000e-01 END PART OF THE WAVEFORM
1 1 1.000e00
1 8.400e-01 4.200e+05
0
4.000e-06
1 1.000e+00 6.790e+05
0
5.19000e-06 2.930795e-05 1e-02 1 1 4.38000e-06 6.00000e-06
7.19000e-06 8.324949e-06 1e-02 1 1 6.38000e-06 8.00000e-06
9.19000e-06 3.114001e-06 1e-02 1 1 8.38000e-06 1.00000e-05
1.11900e-05 1.468999e-06 1e-02 1 1 1.03800e-05 1.20000e-05
1.31900e-05 7.994008e-07 1e-02 1 1 1.23800e-05 1.40000e-05
1.51900e-05 4.845643e-07 1e-02 1 1 1.43800e-05 1.60000e-05
1.71900e-05 3.201334e-07 1e-02 1 1 1.63800e-05 1.80000e-05
1.91900e-05 2.242720e-07 1e-02 1 1 1.83800e-05 2.00000e-05
2.11900e-05 1.642196e-07 1e-02 1 1 2.03800e-05 2.20000e-05
2.36900e-05 1.194221e-07 1e-02 1 1 2.23800e-05 2.50000e-05
2.66900e-05 8.588368e-08 1e-02 1 1 2.53800e-05 2.80000e-05
3.01900e-05 6.296099e-08 1e-02 1 1 2.83800e-05 3.20000e-05
3.46900e-05 4.492492e-08 1e-02 1 1 3.23800e-05 3.70000e-05
4.06900e-05 3.127694e-08 1e-02 1 1 3.73800e-05 4.40000e-05
```



## TTEM, HIGH MOMENT TEM-FILE

```
%tTEM, High moment
72 3
0.00 0.00 -0.50 -9.53 0.00 -0.30
  4 8.00
-02.00 -01.00
  02.00 -01.00
  02.00 01.00
-02.00 01.00
3 3 3
3 1
3 1
43 ... 3.7422e-06 4.5000e-06 6.0000e-03 0.0000e-01 END PART OF THE WAVEFORM
1 1 1.000e00
1 8.400e-01 4.200e+05
0
6.000e-06
1 1.000e+00 6.790e+05
0
9.19000e-06 3.487474e-06 1e-02 1 1 8.38000e-06 1.00000e-05
1.11900e-05 1.603474e-06 1e-02 1 1 1.03800e-05 1.20000e-05
1.31900e-05 8.584445e-07 1e-02 1 1 1.23800e-05 1.40000e-05
1.51900e-05 5.126946e-07 1e-02 1 1 1.43800e-05 1.60000e-05
1.71900e-05 3.329417e-07 1e-02 1 1 1.63800e-05 1.80000e-05
1.91900e-05 2.312006e-07 1e-02 1 1 1.83800e-05 2.00000e-05
2.11900e-05 1.692325e-07 1e-02 1 1 2.03800e-05 2.20000e-05
2.36900e-05 1.218537e-07 1e-02 1 1 2.23800e-05 2.50000e-05
2.66900e-05 8.733728e-08 1e-02 1 1 2.53800e-05 2.80000e-05
3.01900e-05 6.360679e-08 1e-02 1 1 2.83800e-05 3.20000e-05
3.46900e-05 4.555252e-08 1e-02 1 1 3.23800e-05 3.70000e-05
4.06900e-05 3.174452e-08 1e-02 1 1 3.73800e-05 4.40000e-05
4.81900e-05 2.196769e-08 1e-02 1 1 4.43800e-05 5.20000e-05
5.71900e-05 1.514165e-08 1e-02 1 1 5.23800e-05 6.20000e-05
6.86900e-05 1.011344e-08 1e-02 1 1 6.23800e-05 7.50000e-05
8.31900e-05 6.713178e-09 1e-02 1 1 7.53800e-05 9.10000e-05
1.01700e-04 4.500398e-09 1e-02 1 1 9.13800e-05 1.12000e-04
1.25200e-04 2.947764e-09 1e-02 1 1 1.12400e-04 1.38000e-04
1.54200e-04 1.989106e-09 1e-02 1 1 1.38400e-04 1.70000e-04
1.91200e-04 1.366303e-09 1e-02 1 1 1.70400e-04 2.12000e-04
2.37700e-04 9.308418e-10 1e-02 1 1 2.12400e-04 2.63000e-04
2.95700e-04 6.406197e-10 1e-02 1 1 2.63400e-04 3.28000e-04
3.69200e-04 4.129136e-10 1e-02 1 1 3.28400e-04 4.10000e-04
4.61700e-04 2.643683e-10 1e-02 1 1 4.10400e-04 5.13000e-04
5.78200e-04 1.741682e-10 1e-02 1 1 5.13400e-04 6.43000e-04
7.24700e-04 1.089956e-10 1e-02 1 1 6.43400e-04 8.06000e-04
9.09200e-04 7.063410e-11 1e-02 1 1 8.06400e-04 1.01200e-03
```

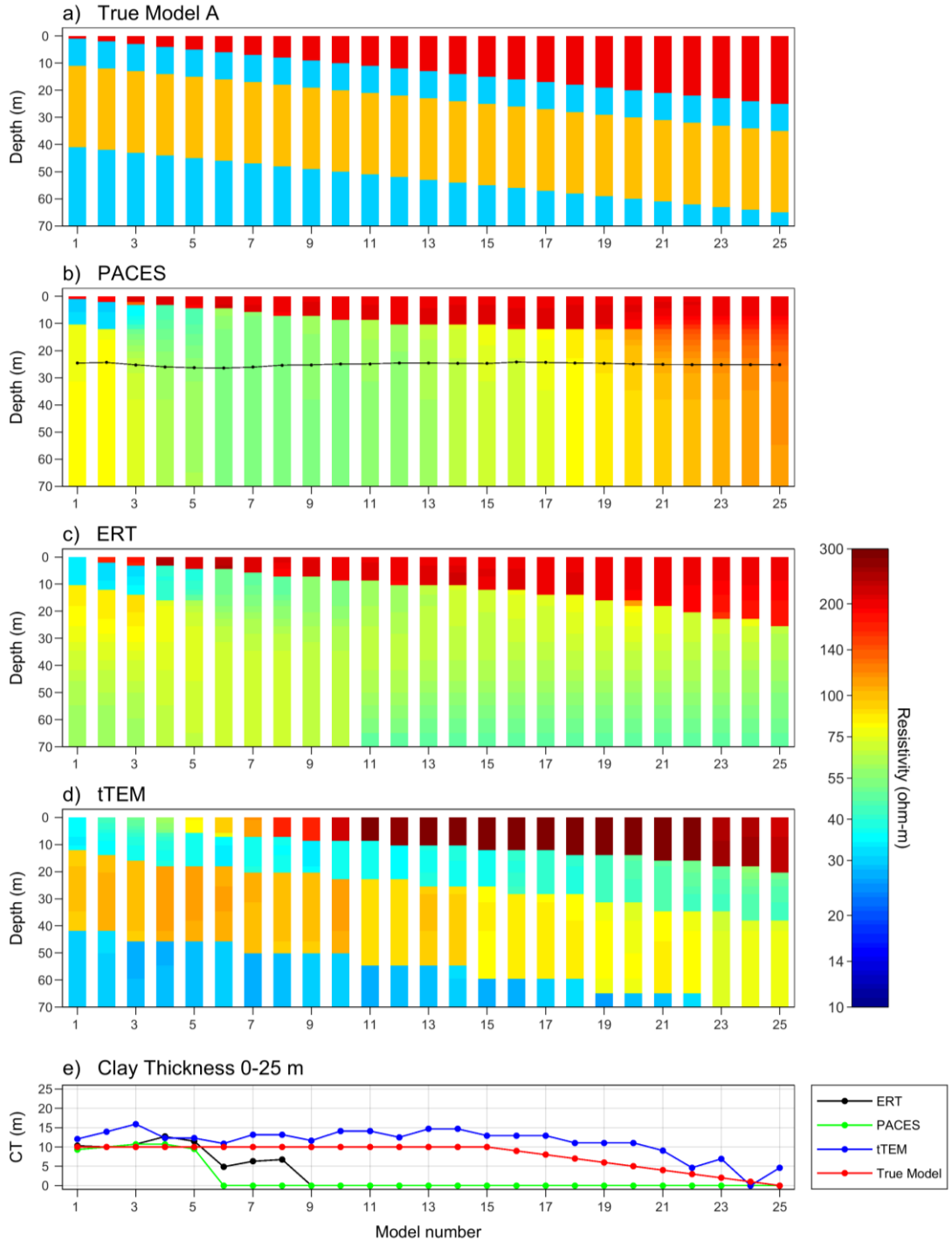


## **APPENDIX 4    ADITIONAL MODEL SWEEPS**

This appendix holds sharp inversion of the model sweeps presented in this section 5.2 (Model sweep A,B,C,D) and additional models sweeps (E,F) with both smooth and sharp inversions. Same plot layout as the in section 5.2.

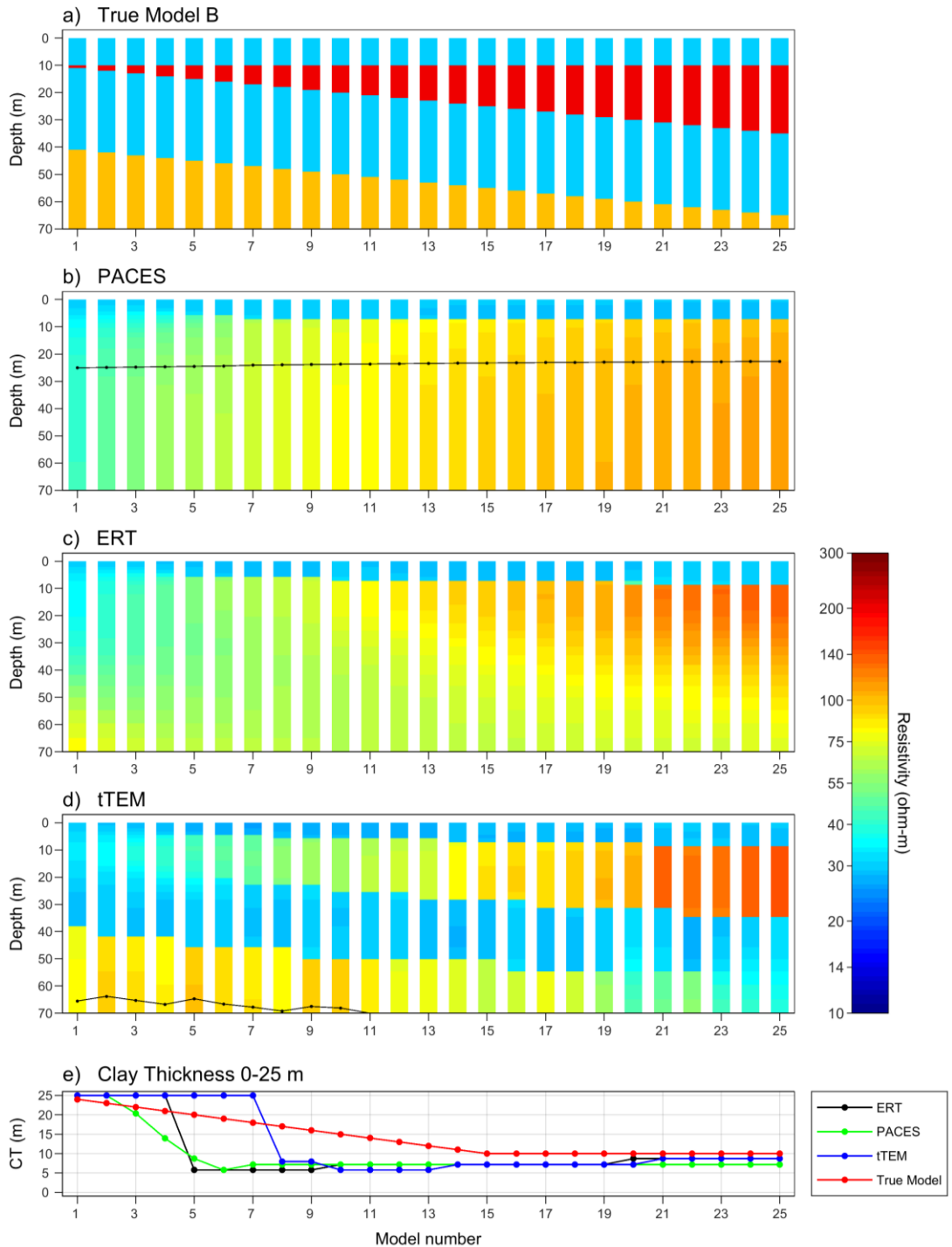


### MODEL SWEEP A - SHARP INVERSION



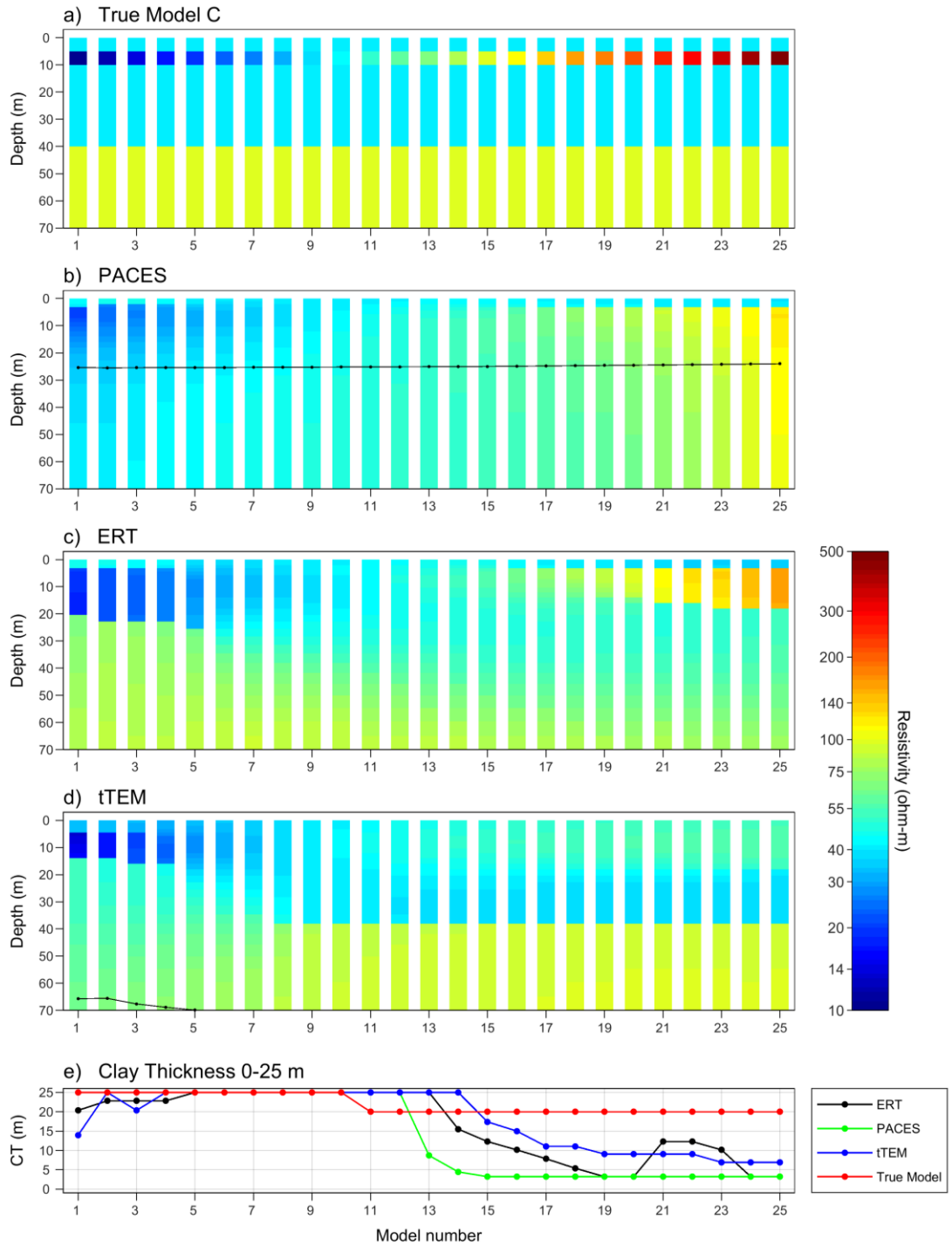


## MODEL SWEEP B – SHARP INVERSION



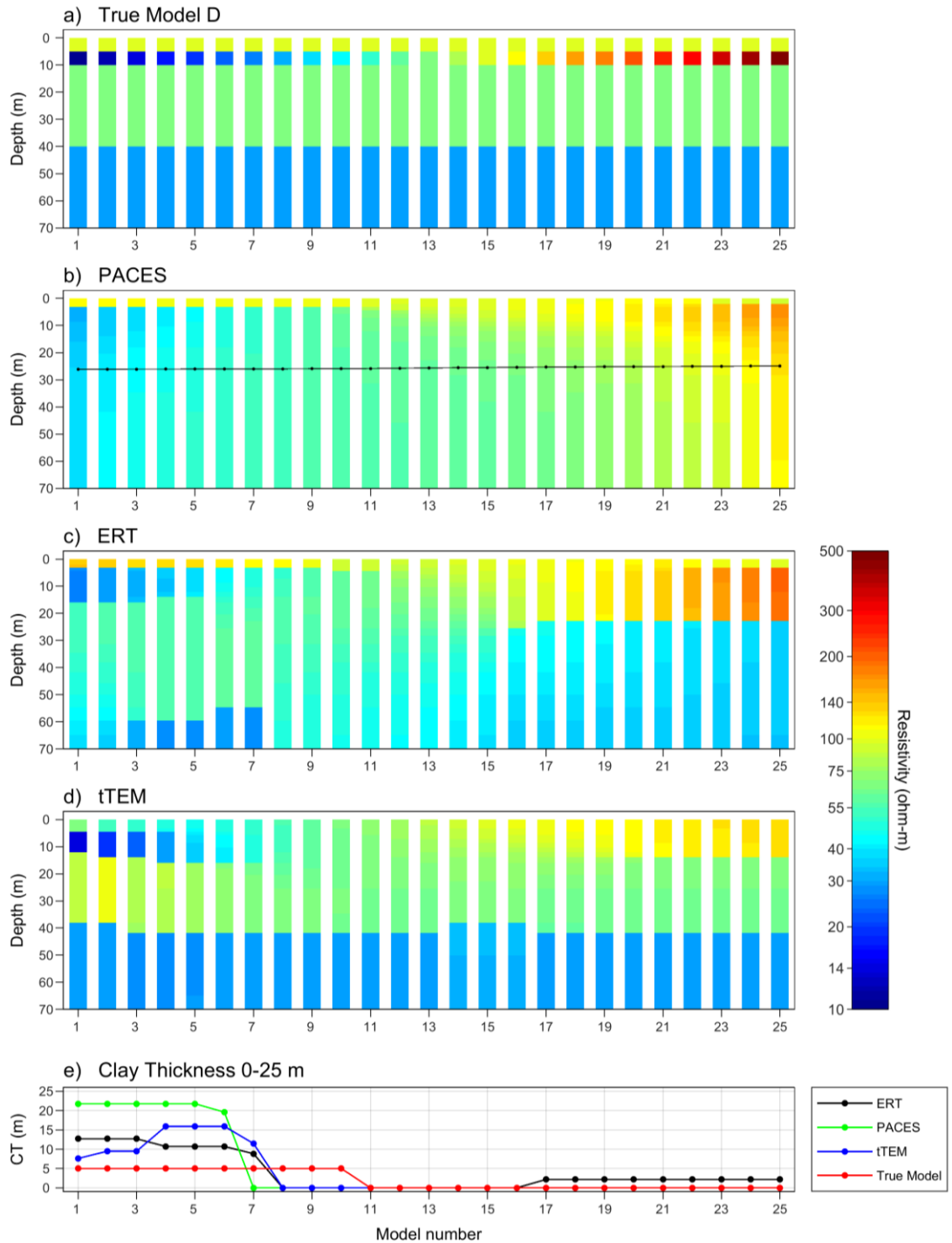


### MODEL SWEEP C – SHARP INVERSION



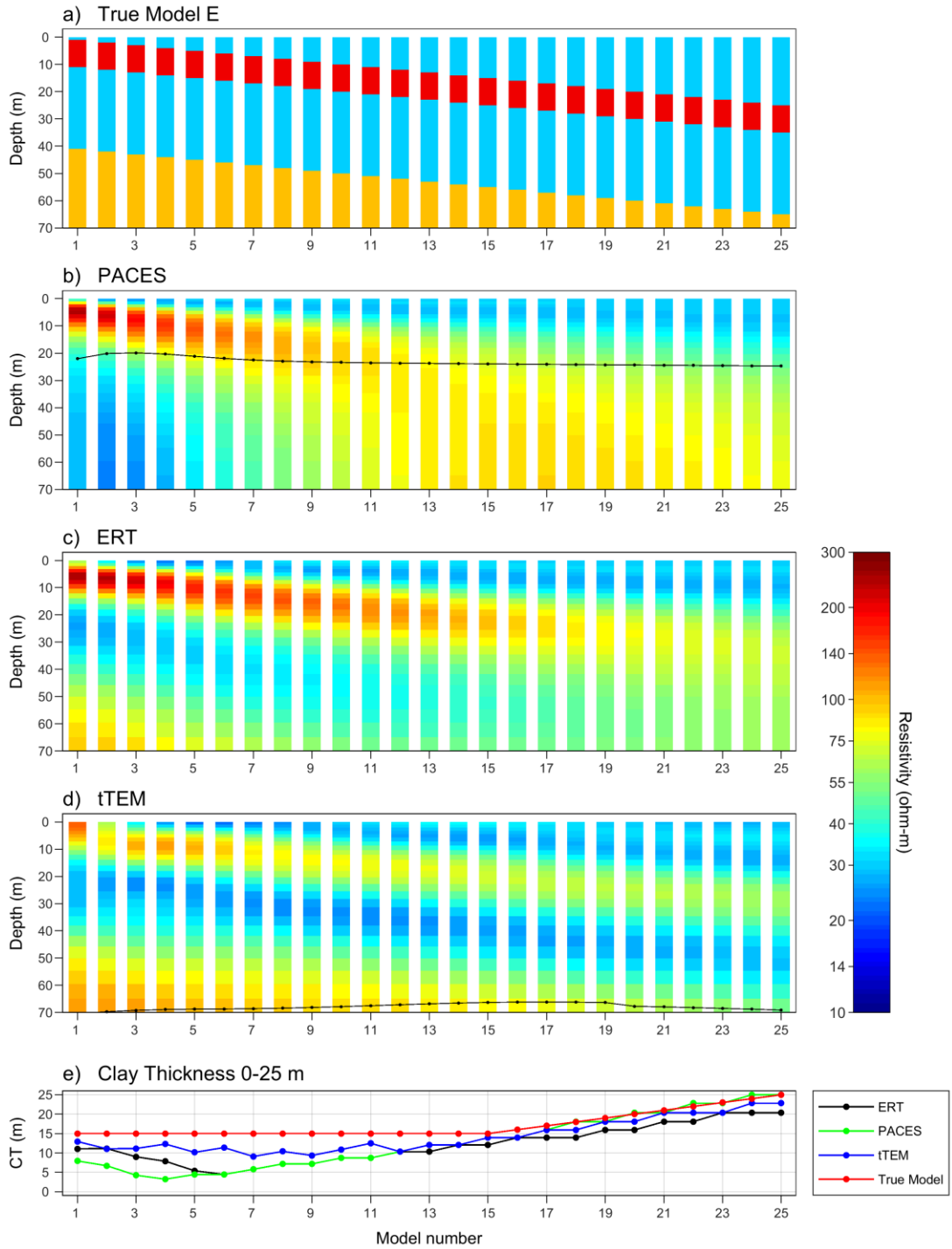


### MODEL SWEEP D – SHARP INVERSION



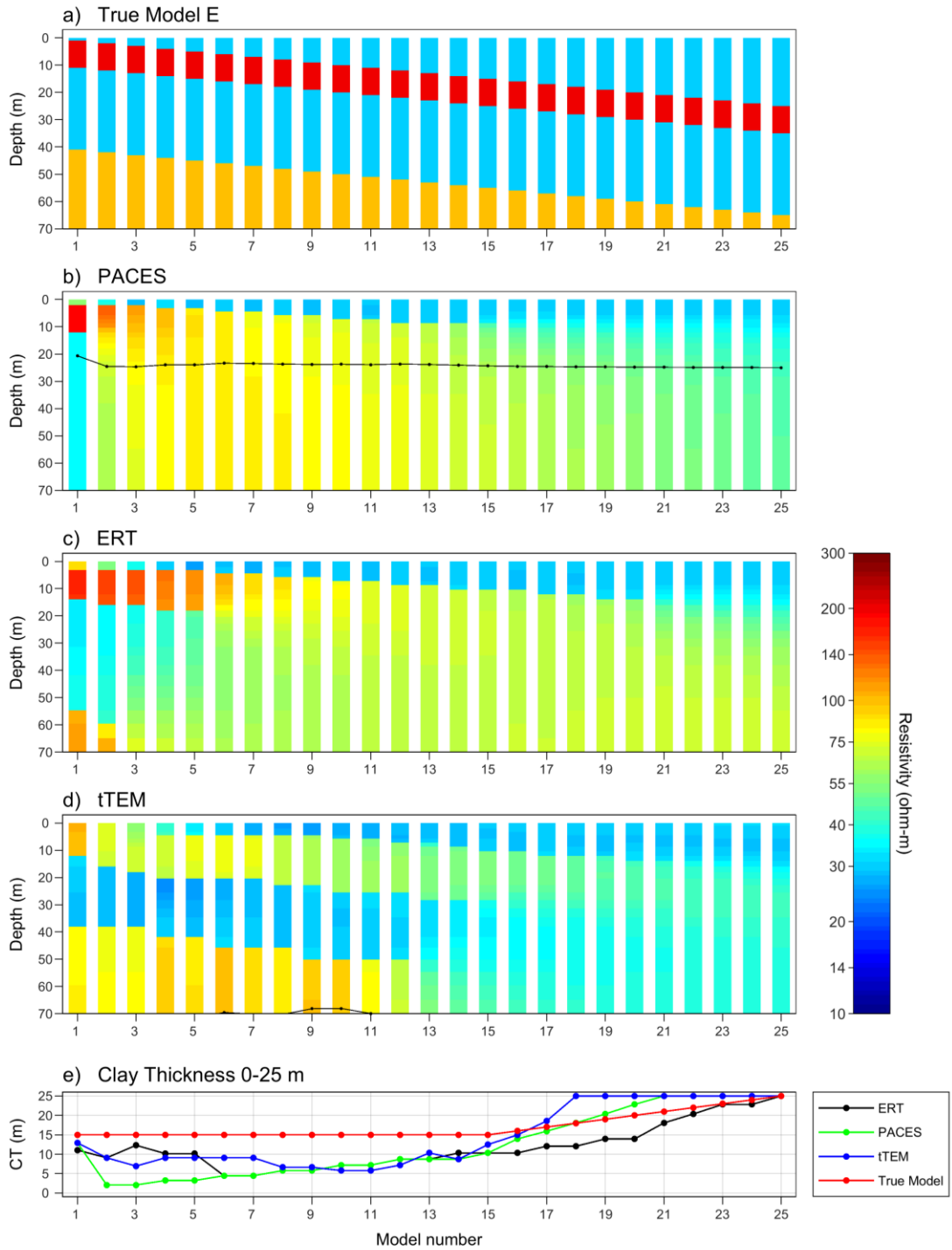


### MODEL SWEEP E – SMOOTH INVERSION



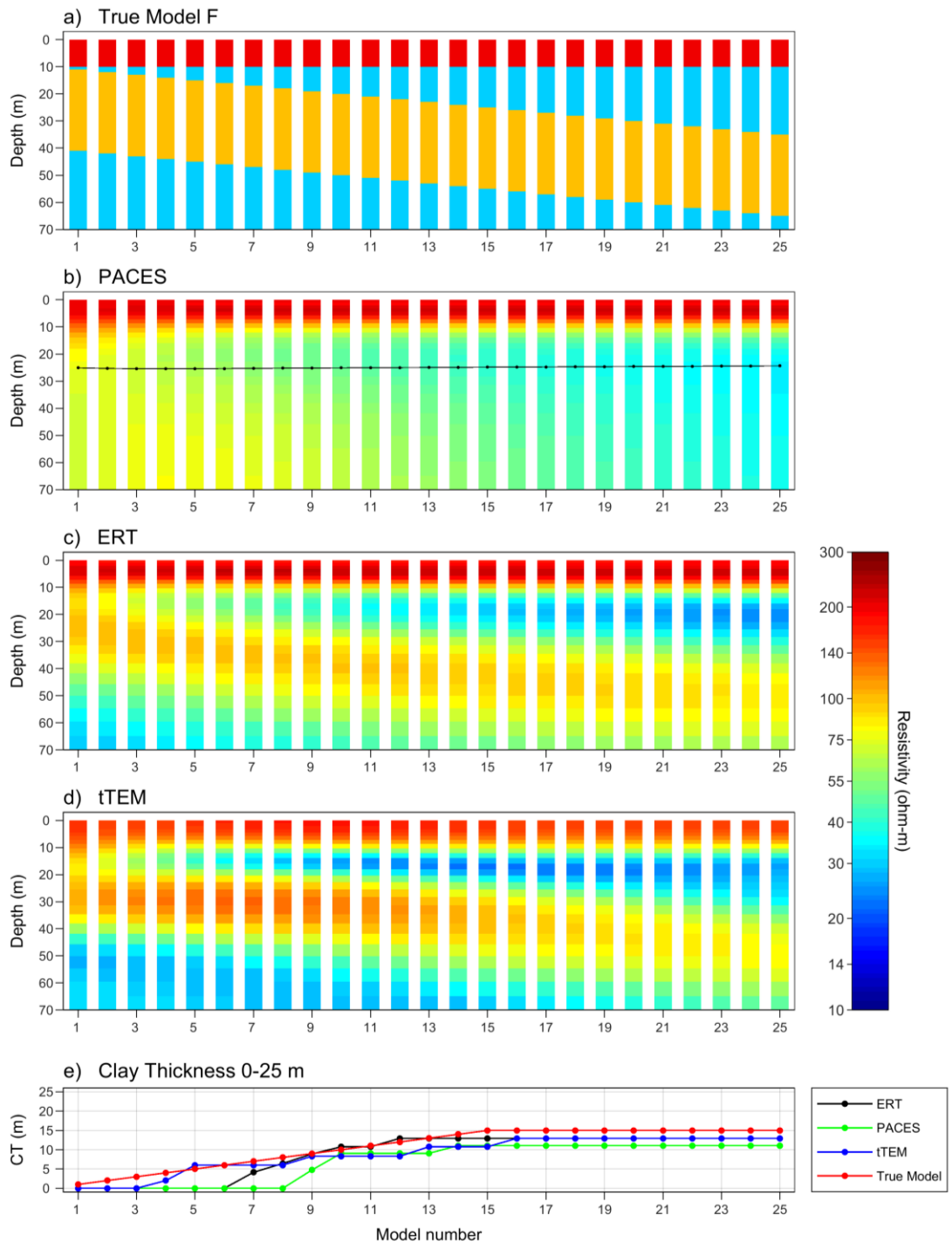


### MODEL SWEEP E – SHARP INVERSION





## MODEL SWEEP F – SMOOTH INVERSION





### MODEL SWEEP F - SHARP INVERSION

